LIMNOLOGY and OCEANOGRAPHY

ASLO

Limnol. Oceanogr. 66, 2021, 366–391

doi: 10.1002/lno.11610

Massive silicon utilization facilitated by a benthic-pelagic coupled feedback sustains deep-sea sponge aggregations

Manuel Maldonado,[1*] **Lindsay Beazley**,[2] **María López-Acosta**,[1] **Ellen Kenchington**,[2] **Benoit Casault**,[2] **Ulrike Hanz**,[3] **Furu Mienis**[3]

[1]Department of Marine Ecology, Center for Advanced Studies of Blanes (CEAB-CSIC), Girona, Spain
[2]Department of Fisheries and Oceans, Bedford Institute of Oceanography, Dartmouth, Nova Scotia, Canada
[3]Department of Ocean System Sciences, NIOZ Royal Netherlands Institute for Sea Research and Utrecht University, Den Burg, The Netherlands

Abstract

Biogeochemical cycling of silicon (Si), largely affected by biological drivers, is pivotal to the ecological functioning of the ocean. Most knowledge regarding biological utilization of Si derives from research on phototrophic organisms circumscribed to the photic ocean (i.e., diatoms). Utilization of Si in the aphotic ocean, where heterotrophic silicifiers become relevant Si users, remains poorly investigated. Here we quantify the flux rates and stocks characterizing Si cycling across dense aggregations of the hexactinellid sponge *Vazella pourtalesii* established in the aphotic zone of the central Scotian Shelf, Nova Scotia, Canada. Although individual rates of silicic acid consumption were low compared to other sponge species and diatoms, the large abundance of individuals (6.5 million) over the extension of these sponge grounds (2105 km^2) leads to massive annual silicic acid consumption, invested in producing their siliceous skeletons of biogenic silica. This sponge activity accumulates large biogenic silica stocks both in the living population and in the sediments. Skeletal pieces in sediment revealed that a good portion of biogenic silica deposited to the bottom after sponge death recycles as silicic acid before being permanently buried. This biogenic silica–silicic acid turnover, facilitated by an unconventional silicification pattern that favors delamination and dissolution of *V. pourtalesii* spicules, causes silicic acid enrichment at oceanographic dimensions in the bottom water of the central Scotian Shelf. Silicic acid efflux from the bottom sustains a feedback mechanism that fulfills sponge needs for silicic acid and facilitates the persistence of sponge aggregations in the long term.

Silicon (Si), in the form of soluble silicic acid, is a key inorganic nutrient in the ocean. Its availability modulates ocean primary productivity (Nelson et al. 1995; Tréguer et al. 1995) and the CO_2 exchange with the atmosphere (Mackenzie and Garrels 1966; Tréguer and Pondaven 2000). Regional patterns of silicic acid availability largely result from the consumption of this nutrient by marine organisms, with diatom utilization in the photic zone among the best known (Nelson et al. 1995; Tréguer et al. 1995). Other marine organisms also consume silicic acid, such as sponges (Maldonado et al. 2012), rhizarians (Llopis Monferrer et al. 2020), choanoflagellates (Marron et al. 2019), silicoflagellates, testate amoeba, chrysophytes (Simpson and Volcani 1981), and cyanobacteria (Baines et al. 2012), but their particular roles in Si cycling remain largely unquantified. Except cyanobacteria, these consumers take up silicic acid and polymerize it as biogenic silica, the fundamental material from which their various types of siliceous skeletons are made.

Because the consumption of silicic acid and the production of biogenic silica by diatoms are activities restricted to the photic ocean, a major gap in knowledge persists relative to the biological silicic acid utilization by non-phototrophic Si consumers in deep water and in disconnection from the CO_2 fixation of photosynthesis. The silica produced by heterotrophic organisms has recently been defined as "dark silica" (Maldonado et al. 2012; Maldonado et al. 2019). The routes

*Correspondence: maldonado@ceab.csic.es

Additional Supporting Information may be found in the online version of this article.

Author Contributions Statement: M.M. conceived this research and assembled the first manuscript, with subsequent help by L.B., M.L.A. and E.K. to refine both tasks. E.K. and L.B. were responsible for organization of the oceanographic cruises and the logistics of fieldwork. L.B. and E.K. developed the spatial modeling and all mapping. B.C. developed silicic acid interpolation layers. F.M. and U.H. were responsible of current meter deployment and analysis of hydrographic data. M.M. conducted the scanning electron microscopy study. M.L.A. and M.M. were responsible for the analysis of sponge morphometry and the quantification of silica in sediments. M.M. and M.L.A. conducted and integrated the global statistical analyses and assembled the cycle model.

through which dark silica flow in the marine system are still poorly understood, particularly in the deep ocean, where highly silicified sponges may form impressive aggregations (Maldonado et al. 2017) suspected to process large amounts of benthic silicon.

To date, only one study has attempted to complete the Si cycle in a deep-water sponge aggregation: the Pacific reef system of hexactinellid sponges established on the deep shelf (84–164 m) of the Strait of Georgia, British Columbia, Canada (Chu et al. 2011). However, this is a singular and unique type of sponge-dominated deep-sea system, the Si cycle of which cannot be extrapolated easily to other sponge aggregations. The sponge reefs grow because, unlike in most other sponge aggregations, the siliceous pieces of the skeleton of the individuals are not separable but fused to each other in impressive silica networks (Chu et al. 2011). Those silica frameworks remain in place after sponge death and experience little dissolution over time, becoming a suitable hard substrate for the settlement of subsequent sponge generations. Some of the skeletal frameworks at the base of the sponge reefs have been dated to 10,000 years old and still withstand dissolution. Although some families of hexactinellids and some lithistid demosponges also have skeletons in the form of silica networks, the siliceous skeleton of the majority of sponges consists of independent pieces assembled together through the gluing of collagenous materials. Once the sponges die, their skeletal pieces disaggregate and are delivered to the sediment, where they may remain in large patches before being slowly transported horizontally (Bett and Rice 1992; Laguionie-Marchais et al. 2015), depending on the environments. Because the silica of sponges is relatively resistant to dissolution in seawater (compared to that of diatoms), sponge-dominated communities are often seen as important Si sinks (Maldonado et al. 2005; Chu et al. 2011; Maldonado et al. 2019). However, the resistance to dissolution of only some hexactinellid species has recently been reported—not without controversy—to be minimal (Bertolino et al. 2017) compared to that of most other sponges assayed to date (Kamatani 1971; Maldonado et al. 2005; Maldonado et al. 2019). The varying resistance to dissolution of the different "types" of sponge silica may have important implications to the turnover between biogenic silica production and silicic acid recycling in the dark ocean, where sponge aggregations can become relevant Si users.

The current study, framed within the European Union H2020 project SponGES, investigates Si cycling in aggregations of the rosellid hexactinellid *Vazella pourtalesii* (Schmidt, 1870). This northwest Atlantic species forms extensive monospecific aggregations (Fig. 1A,B) on the continental shelf off Nova Scotia, Canada (Fig. 1C), at depths from ~ 160 to 200 m (Beazley et al. 2018). These aggregations will be referred to as "*Vazella* grounds" henceforth. Using a remotely operated vehicle (ROV), we documented the natural densities and morphometry of *V. pourtalesii* (Fig. 2A–C), modeling biomass distribution across the extension of the *Vazella* grounds on the Scotian Shelf. The silicic acid distribution in demersal water and its availability to the sponges were also modeled and, through a kinetic equation developed elsewhere (Maldonado et al. 2020) to predict the silicic acid utilization rate by *V. pourtalesii* as a function of the silicic acid availability, the annual silicic acid consumption was scaled up to the sponge ground level. Additionally, through a quantitative determination of *V. pourtalesii* silica in sediments collected from the sponge grounds, rates of deposition, burial, and recycling of sponge biogenic silica were estimated. With these elements, we propose a comprehensive model that budgets Si masses and flux rates through the *Vazella* grounds, highlighting their ecological and biogeochemical significance. Our study provides a case for the vast benthic aphotic environment and potentially similar sponge grounds that often occur elsewhere in the deep sea.

Materials and methods

Species habitat

V. pourtalesii is distributed along the eastern seaboard of North America, with specimens reported on the continental shelf and slope off both Florida and Nova Scotia (Canada), across a depth range of ~ 100–750 m (Reiswig 1996; Tabachnick 2002; Beazley et al. 2018). In Emerald Basin, a deep-water (> 200 m) basin situated on the central Scotian Shelf, this species forms extensive monospecific aggregations consisting of an abundance of vase-shaped individuals measuring up to about 40 cm in height (Fig. 1A,B; Supporting Video S1). In 2013, Fisheries and Oceans Canada closed two areas encompassing some of the densest sponge grounds formed by *V. pourtalesii* to all bottom fishing activities (Fig. 1C): the Emerald Basin Sponge Conservation Area (195 km^2) and the Sambro Bank Sponge Conservation Area (62 km^2). These two sponge conservation areas are often referred to hereafter as "sponge closures."

Sponge collection

Individuals of *V. pourtalesii* were collected from the sponge grounds of Emerald Basin to determine body volume and other morphometric parameters. Collection was accomplished during two multidisciplinary oceanographic missions held in 2016 and 2017. In August 2016, Oceaneering's "Spectrum" ROV (https://www.oceaneering.com/datasheets/ROV-Spectrum.pdf), a light duty, work-class, cage-tethered ROV was deployed from the Canadian Coast Guard Ship *Hudson* to collect live sponges from the sponge grounds located in Emerald Basin Sponge Conservation Area (Fig. 1C). Details of sample locations and associated environmental data collection (e.g., CTD and box cores) are reported in Kenchington et al. (2017). In September 2017, the ROV "ROPOS" (https://www.ropos.com/)

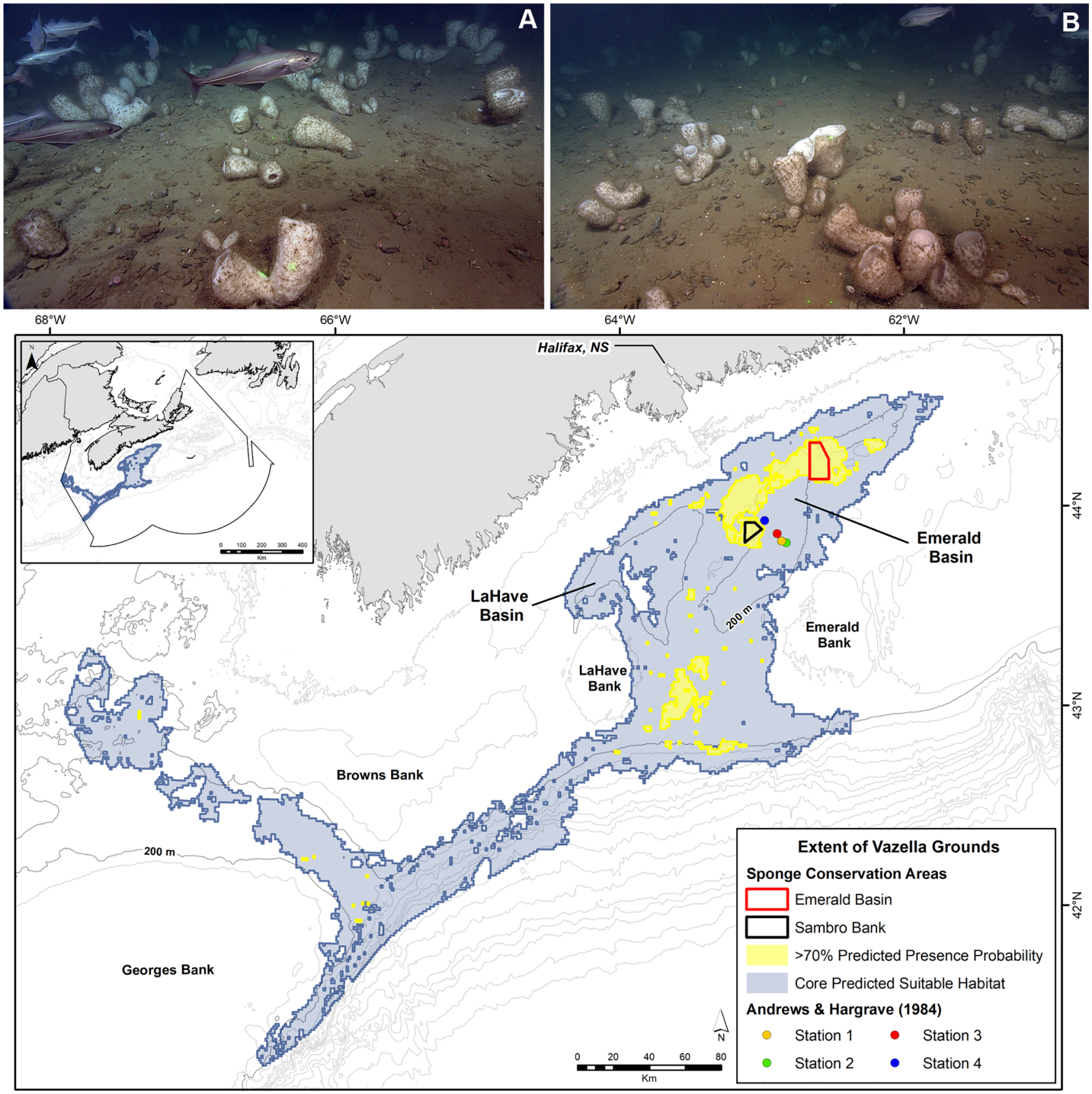

Fig 1. (**A** and **B**) Depiction of the *Vazella* grounds at Sambro Bank Sponge Conservation Area (Emerald Basin, Scotian Shelf). Note the general sponge abundance, along with the virtual absence of decaying individuals and numerous small, young individuals. (**C**) Spatial extent of the *Vazella* grounds, i.e., those areas predicted with > 70% presence probability from Beazley (2018). Also shown are Fisheries and Oceans Canada's two sponge conservation areas, and the area of predicted suitable habitat from Beazley (2018). Location of Stations 1–4 sampled by Andrews and Hargrave (1984) to determine silicic acid concentrations in pore water and silicic acid efflux from the sediments to the bottom water.

was deployed from the Canadian Coast Guard Ship *Martha L. Black* in Sambro Bank Sponge Conservation Area (Fig. 1C); see Beazley et al. (2017) for details.

A total of 34 sponge individuals were collected across both years using the manipulator arms of the ROVs and transported to the surface in a covered "biobox." Once onboard, live sponges

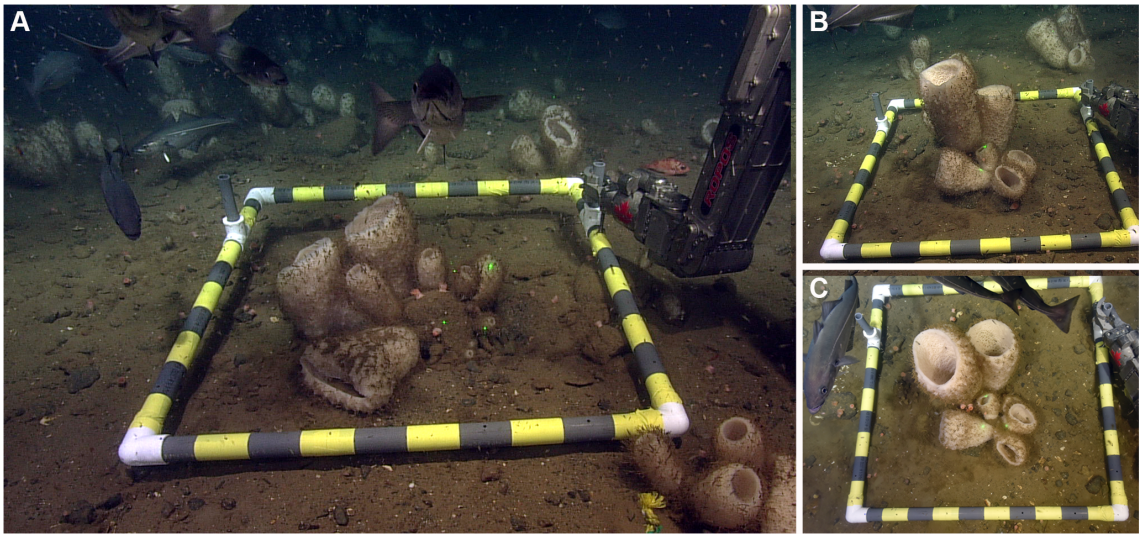

Fig 2. (**A**) General view of the sponge community and the ROV deploying a 1 × 1 m measuring frame (quadrat) to estimate sponge density and individual biomass. (**B** and **C**) Examples of view pairs—i.e., nearly parallel (**B**) and nearly perpendicular (**C**) to the bottom used for each quadrat to estimate the morphological parameters of each sponge (i.e., height, maximum width, width at the base, etc.).

were transferred to an insulated 500-liter polyethylene holding tank inside a refrigerated container (see Methods S1). Upon return to the Bedford Institute of Oceanography in Dartmouth, Nova Scotia, the live sponges were transferred to a 500-liter aquarium and processed further for morphometric analysis.

Sponge morphometry

For the 34 collected sponges, volume was estimated by water displacement. Total height, maximum width, basal body width, width of the atrium, length of the atrium, and average thickness of the body wall were also measured. We did not consider osculum diameter, as it can be contracted or extended to a different degree depending on the physiological state of the sponges. The pairwise relationships between the various morphometric parameters were explored by regression analyses to identify relevant equations that would allow us to reconstruct volume reliably from the linear morphometric parameters obtained from video footage and digital still images collected in situ.

When sponge height was greater than 5 cm, sponge shape was approximated to that of a solid truncate cone (*vol 1*) and then volume of the internal, hollow atrium (*vol 2*) was detracted, which had also been calculated as a truncate cone (see Fig. S1). Sponge volume (*Vol*) was then calculated as:

$$Vol = vol\,1 - vol\,2$$

being,

$$vol\,1 = 1/3 \times \pi \times h \times \left(\tfrac{1}{2}w^2 + \tfrac{1}{2}bw^2 + ((\tfrac{1}{2}w) \times (\tfrac{1}{2}bw))\right)$$

$$vol\ 2 = 1/3 \times \pi \times ah \times ((\tfrac{1}{2}\ w) - wt)^2 + (\tfrac{1}{2}\ (wb - wt))^2 + ((\tfrac{1}{2}\ w) - wt) \times (\tfrac{1}{2}\ (wb - wt)))$$

where "*h*" is height of the sponge, "*w*" maximum width, "*bw*" width of the body at the base, "*wb*" body diameter at the level of the atrium bottom, "*wt*" thickness of the body wall at the mid portion of the atrium, and "*ah*" atrium height. Interestingly, *ah* was also empirically corroborated to be "$ah = h - (1.5\ wt)$". When the sponges were less than 5 cm in height, their shape approximated better to a cylinder than to a truncate cone, and body volume was calculated as that of a solid cylinder minus that of an internal atrial cylinder. We also examined the error between the volume value when morphometrically estimated through the cone or cylinder formulas and when measured by water displacement.

The sponges were then wet weighed (g), dried at 60°C to a constant dry weight (g), and combusted at 540°C for 10 h for ash-free dry weight (g). The biogenic silica content was estimated as 95% of the ash weight. However, for comparative purposes, the biogenic silica content of some of the sponges was also estimated through the loss of weight before and after desilicification of the sample in 5% hydrofluoric acid (Maldonado et al. 2005). The pairwise relationship between the dry weight vs. volume and that between biogenic silica content vs. volume were explored in order to obtain equations to estimate biogenic silica contents from volumetric estimates obtained from the ROV digital images and video frames (see below).

Estimation of biogenic silica stock in *Vazella* grounds

During the ROPOS 2017 mission to the Sambro Bank Sponge Conservation Area, forward- and downward-facing video footage of the seabed was collected to document the fine-scale distribution and natural density of *V. pourtalesii*. Density of the sponges was estimated across two different spatial scales. In the first approach, a 1 × 1 m PVC quadrat was

placed on the seabed (n = 32) every 10 m along a transect in an orthogonal east–west pattern across the sponge grounds. Digital images of each quadrat and surrounding habitat were collected (Fig. 2A–C). We enumerated the sponges in each quadrat through the simultaneous recording of both the forward- and downward-facing video cameras to obtain number of individuals per square meter (i.e., density). From the digital images we also obtained the necessary morphometric parameters from each sponge individual to reconstruct its volume, organic dry weight and biogenic silica content through a variety of morphometric relationships.

As *V. pourtalesii* may form clumps that lead to an aggregated distribution over spatial scales larger than 1 m^2, a second approach was used to estimate sponge density. In this approach, a single video transect of approximately 202 m in length was collected using ROPOS in a north–south direction in the Sambro Bank Sponge Conservation Area. Video collection was made with ROPOS in "Transect Mode," where the forward velocity (mean ± SD: 0.13 ± 0.03 knots) and altitude (mean ± SD: 1.01 ± 0.23 m) above bottom were kept relatively constant as the vehicle traversed towards the end waypoint. The total area of seabed surveyed across this linear transect was 468 m^2. To facilitate counting and measuring individuals of *V. pourtalesii* from the continuous video, frame grabs of all visible individuals were extracted from the downward-facing video camera using the "Capture Window Control" tool of the graphic design software PicPick (version 5.0.2). From the video, a frame grab was taken of each sponge at an angle that facilitated its measurement. Frame grabs were processed in Adobe Photoshop CC 2017 and all *V. pourtalesii* individuals were enumerated from each. Using the "Ruler Tool" in Photoshop, the length (height) and maximum body width of each sponge were measured in pixels and converted to cm using the 10 cm scaling lasers in each frame grab. From here, an average number of individuals per square meter (with no associated error calculation) was derived. Likewise, the volume (mL) of each individual across the transect extension rendered a mean sponge biomass (mL) per m^2, but without associated error. The average sponge density and biomass resulting from the quadrat and the transect approaches were compared.

The resolution and orientation of the digital images and video frame grabs often prevented the estimation of all relevant linear morphometric parameters needed to estimate the volume of the individuals using the truncate-cone formulas. Therefore, as indicated in the results, significant relationships between total height and maximum body width vs. volume were developed, assuming that both relationships have the shared constraint that maximum volume in the population is < 15 liter. Because those relationships were strong and highly significant, we estimated the volume of the sponge individuals found in the digital images and transect from both their length and maximum width, and then averaged those two volume values to obtain the final volume of each individual.

The area occupied by the *Vazella* sponge grounds on the Scotian Shelf was estimated by applying a threshold criterion to modeled presence probability outputs from Beazley et al. (2018). Figure 1C shows that while the two conservation areas (Emerald Basin and Sambro Bank Sponge Conservation Areas) encompass the large majority of those areas predicted with the highest probability of occurrence (95%), they do not fully encompass them, and significant concentrations of *V. pourtalesii* as defined by kernel density estimation analysis using biomass catch data (Kenchington et al. 2016) remain unprotected outside (Beazley et al. 2018). Therefore, the extension of the sponge grounds was instead identified by applying a 70% threshold to the presence probability surface of Beazley et al. (2018) generated from random forest modeling using presence/absence data (see Methods S2). This area is 2104.6 km^2 in size and encompasses the large majority of occurrences in the upper Scotian Gulf and on the saddle between LaHave and Emerald Banks in the lower Scotian Gulf, also including small, localized patches of higher presence probability in the Northeast Channel and Gulf of Maine (Fig. 1C).

Using ArcMap version 10.6.1., the 1 × 1 km raster grid containing all predicted presence probabilities of *V. pourtalesii* from > 70% to 100%, displayed in 5% equal presence probability intervals in Beazley et al. (2018), was converted to a polygon layer of 1 × 1 km cells, each representing a given presence probability. The total area encompassed by all cells with probability values within each 5% probability interval (six intervals from > 70% to 100%) was calculated. In order to convert presence probability into sponge density, the average density obtained by the quadrat approach was then multiplied by the mid-point of each 5% presence probability bin to obtain a weighted estimate of density for areas predicted with successively lower presence probabilities. As our empirical determinations of sponge density were obtained for spatial cells of 0.975 presence probability, we multiplied the average density of sponges per 1 m^2 quadrat of 3.78 ind. m^{-2} per 0.975 presence probability to obtain an average density of 3.69 ind. m^{-2} across cells with > 95% to 100% presence probability. This process was repeated across the spatial cells with decreasing presence probability. Here, we assumed and later confirmed that the relationship between density and presence probability is linear, and that higher-probability areas equate to areas where the habitat is more suitable and would thus accommodate more individuals, compared to lower-probability areas.

Finally, in order to convert presence probability into sponge volume as required for successively estimating the biogenic silica stock and silicic acid utilization across the *Vazella* grounds, the average sponge volume obtained by the quadrat approach was multiplied by the mid-point of each 5% presence probability bin. This procedure yielded a weighted estimate of biomass (in volume), and through empirically

Table 1. Summary of morphometric features for the 34 collected individuals of *V. pourtalesii*, including total height, maximum body width, body wall thickness at the mid length of the atrium, body volume calculated by water displacement, and estimated through the morphometric approaches, dry weight, and biogenic silica (BSi) content estimated as either 95% of ash weight or through desilicification in hydrofluoric acid (HF). See section "Methods".

Sponge code	Heigth (cm)	Max width (cm)	Wall thickness (cm)	Displaced vol. (mL)	Estimated vol. (mL)	Dry weight (g)	BSi content (g)	
							HF	Ash
2016-1	14.1	7.9	1.6	365.3	321.0	22.9	18.5	16.6
2016-2	15.2	6.7	1.2	267.5	221.9	18.9	13.7	–
2016-3	13.9	7.8	1.2	298.6	–	22.9	18.1	–
2016-4	14.5	6.5	1.2	222.0	–	13.7	14.1	–
2016-5	12.2	6.0	1.2	217.9	186.6	18.9	17.5	14.8
2016-6	13.6	5.9	1.1	181.3	145.2	14.3	16.3	-
2016-8	11.7	7.1	1.2	263.2	281.1	17.2	17.5	17.2
2016-9	15.6	6.8	1.2	217.4	231.3	15.8	14.7	–
2016-10	12.0	4.7	1.2	123.0	–	8.1	8.0	–
2016-11	11.0	5.4	1.0	117.9	–	8.2	6.1	–
2016-12	15.2	7.0	1.2	257.7	251.8	18.0	17.0	–
2017-2	9.0	4.1	1.0	81.0	80.2	3.6	–	–
2017-3	10.6	4.8	1.3	191.0	177.4	9.9	–	–
2017-4	11.2	4.4	1.2	136.0	139.6	6.8	–	–
2017-5	10.9	5.6	1.3	141.0	146.9	7.5	–	–
2017-6	6.5	4.0	1.0	61.0	68.2	4.8	–	–
2017-8	7.2	4.4	0.9	71.0	75.3	3.6	–	–
2017-9	9.8	5.2	1.1	111.0	129.9	7.4	–	–
2017-10	9.1	4.6	1.0	81.0	92.4	3.7	–	–
2017-11	6.6	3.1	0.9	41.0	36.5	2.2	–	–
2017-12	8.6	4.4	1.1	81.0	91.4	4.2	–	–
2017-13	7.1	3.3	0.9	51.0	53.1	2.6	–	–
i 1-1-2_a	17.0	9.7	1.7	681.3	761.4	37.2	–	–
i 1-1-2_b	3.1	1.5	0.2	3.0	2.8	-	–	–
i 1-5-6	10.9	6.0	1.3	169.0	169.1	7.8	–	–
i 2-1-2	14.2	7.4	1.4	440.0	477.6	19.5	–	–
167 - 4y	13.3	5.1	1.5	175.0	162.9	7.5	–	5.5
169A - 4y	10.0	6.3	1.1	130.0	120.7	4.6	–	3.3
169B - 4y	13.3	7.6	2.1	210.0	183.9	10.7	–	7.8
167 - 1y	1.5	1.0	0.3	1.0	1.0	0.0	–	0.0
169 - 1y	2.2	1.6	0.3	3.0	3.0	0.1	–	0.1
Mooring A - 1y	2.2	1.1	0.2	–	–	0.1	–	0.1
Mooring B - 1y	1.8	0.9	0.2	–	–	0.1	–	0.0
Mooring C - 1y	0.7	0.5	0.2	–	–	0.0	–	0.0

obtained conversions (see Table 1), it also yielded the biogenic silica stock and silicic acid consumption for areas predicted with successively lower presence probability within the sponge grounds.

Availability of silicic acid to the sponges

Silicic acid concentrations in the bottom layer and at mid depths at discrete (point) locations across the Scotian Shelf between 1990 and 2018 were obtained (see Methods S3) from Fisheries and Oceans Canada's BioChem database (https://www.dfo-mpo.gc.ca/science/data-donnees/biochem/index-eng.html). Data from within 6 m of the seabed were extracted in order to represent silicic acid concentration in demersal water. This resulted in a total of 3287 silicic acid records for interpolation (Fig. S2 A, C). Data on silicic acid concentration at mid depths (50% of water column height ± 5%) in water column of the continental shelf were also selected for the same time period (Fig. S3A,C).

Continuous surfaces of both bottom and mid-depth silicic acid concentration by season for the entire Scotian Shelf were generated using the optimal estimation technique (Petrie

et al. 1999; Johnson et al. 2017). Three nearest neighbors were chosen over which to interpolate the silicic acid data, with data near the interpolation grid point weighted proportionally more than those farther away, following the weighting scheme described in Petrie and Dean-Moore (1996). Interpolations were done by season, where winter = January to March (661 and 246 records for bottom and mid depths, respectively), spring = April to June (364 and 790 records for bottom and mid depths), summer = July to September (2030 and 946 records for bottom and mid depths), and fall = October to December (232 and 682 records for bottom and mid depths). Interpolations were done over a fixed grid equal to the 1×1 km grid of the *V. pourtalesii* presence probability raster from Beazley et al. (2018). As the results of optimal estimation depend strongly on the distribution of data and density of observations (Petrie et al. 1999), interpolations for spring and fall, which were based on low number of observations, particularly for bottom water, were disregarded and only the interpolated surfaces for summer and winter silicic acid were considered.

In order to determine the silicic acid concentration over the sponge grounds, the average values of interpolated summer and winter silicic acid within each 1×1 km grid cell were extracted and matched to their respective predicted presence probability values. For each 5% presence probability interval, the area encompassed by successive silicic acid concentrations binned into 5-μM intervals (e.g., 0–5, 5–10 μM, etc.) was calculated. Interpolated surfaces were displayed as rasters classified into 5-μM intervals. The error associated with the optimal estimation of silicic acid was also produced for each 1×1 km grid cell for both seasons and positions in the water column as an indicator of the relative error of the interpolation across the study extent. This error field is based on the measurement of uncertainty provided with the observations (0.05 μM Si was estimated for this study) and depends on both the form of the correlation function and spatial/temporal distribution of observations (Petrie et al. 1999). Areas with a low number of observations typically result in higher error. In addition to these error plots, the distribution of CTD stations used in each interpolation were also generated to aid in interpretation of the error plots and spatial accuracy of the interpolated surfaces.

As a second approach for comparative purposes, we also calculated the average silicic acid availability to the sponge grounds over the year cycle from literature data (Petrie et al. 1999), which summarize over four decades of weekly to monthly records of average, minimum, and maximum silicic acid concentration in the deep waters (100–275 m) of the central Scotian Shelf (43–45°N, 62–64°W).

Silicic acid consumption by live sponges

A physiological kinetic model specifically developed elsewhere (Maldonado et al. 2020) for *V. pourtalesii* allowed us to estimate herein the rate of silicic acid utilization (μmol Si mL^{-1} sponge h^{-1}) by the sponges in the aggregation as a function of silicic acid availability in seawater (μM) and sponge volume (in mL). The model (r^2 = 0.897, p = 0.001) takes the form of an exponential rise to a maximum (asymptotic) silicic acid consumption velocity (V_{max}) of 0.093 μmol Si mL^{-1} sponge h^{-1}, following the equation:

$$\text{Silicic acid consumption rate per milliliter of sponge} = 0.093 \times \left(1 - 0.978^{DSi}\right),$$

where "*DSi*" represents the concentration of silicic acid (in μM) in the seawater around the sponges.

To estimate annual silicic acid consumption by the sponge grounds, we used two different approaches. First, the kinetic equation was applied to the intersections between the cells of sponge volume and the cells of bottom silicic acid concentration from the spatial interpolated layers for both summer and winter. For an annual reconstruction, it was assumed that 6 months were under summer conditions and 6 months under winter conditions. In a second approach, the kinetic equation was used to estimate the annual silicic acid consumption by each sponge in each of the 32 quadrats analyzed at Sambro Bank Sponge Conservation Area. In this approach, a fixed value of silicic acid availability to the sponges over the year cycle was considered, the one resulting from the decadal silicic acid concentration average for the deep water of the central Scotian Shelf, following data in Petrie et al. (1999). Then, the obtained average (± SD) consumption (g Si m^{-2} yr^{-1}) was extrapolated across the cells of presence probability in the sponge ground extent.

Sponge biogenic silica in sediments: Dissolution, preservation and reservoirs

Using a push corer operated by the ROV ROPOS, we collected a 25 cm sediment core from Sambro Bank Sponge Conservation Area (Video S2). Sediment was sampled from the 1-cm thick uppermost layer and at 23-cm deep. Three sediment subsamples of 10 mg each from both levels were processed to quantify the sponge biogenic silica in form of spicules or spicule fragments, following methods described in Maldonado et al. (2019).

A variety of sedimentological studies based on microfossil taxonomy and/or ^{14}C dating has agreed that the sediment accumulation rate at the central Scotian Shelf ranges minimally (from 0.3 to 0.4 mm yr^{-1}) and that the rate has been essentially constant during the last 10,000 years (Scott et al. 1984; Piper and Fehr 1991; Keigwin et al. 2003). By combining those deposition rates (n = 4; 0.30, 0.334, 0.34, 0.352 mm yr^{-1}), we obtained an average rate of 0.332 mm yr^{-1} with an associated error of 0.022. To be conservative in sediment dating, we rounded those figures to a single decimal, applying to our calculations a mean deposition rate

of 0.3 ± 0.0 mm yr^{-1}, which involved negligible cascading effect in error propagation.

Sediment mass per volume unit was obtained from the wet bulk density through Tenzer and Gladkikh's regression equation (Tenzer and Gladkikh 2014),

$$\rho\,(\mathrm{D}) = [1.66 \pm 0.02] - D \times \left[(5.1 \pm 0.5) \times 10^{-5}\right],$$

where "ρ" is density in g cm^{-3}, "D" is ocean depth in m, "1.66" is the nominal sediment density of the upper sedimentary layer at sea level, and "5.1×10^{-5}" is a coefficient reflecting that density decreases proportionally (relative to the nominal value) at a rate of -0.051 g cm^{-3}.

To calculate the biogenic silica stock buried in the sediments of the sponge grounds several assumptions were made. Numerous studies indicate that the biogenic silica dissolves partially during its burial process, causing the silicic acid concentration of the interstitial water to increase progressively with sediment depth until reaching an asymptotic concentration value, which is attained from 5- to 10-cm burial depth in most sediment types (Hurd 1973; Van Cappellen and Qiu 1997). Previous studies of the sediment at locations of Emerald Basin (Fig. 1C) adjacent to our own study sites indicated that asymptotic silicic acid concentrations are attained at sediment depths shallower than 12 cm and that asymptotic silicic acid concentrations in pore water range from 80 to 340 μM, depending on site (Andrews and Hargrave 1984). Therefore, we assumed that the interstitial water has minimal capacity to further dissolve the sponge biogenic silica buried below 12.5 cm. This sediment depth was taken as the local preservation threshold where sponge opal A (of amorphous, non-crystalline atomic structure) starts progressively becoming opal CT (of microcrystalline organization), and eventually chert by diagenesis. The loss of sponge biogenic silica by dissolution during the burial from the superficial sediment to 12.5 cm can be estimated as

$$\mathrm{BSi}_{\mathrm{pre}\,"i"} = \mathrm{BSi}_{\mathrm{pre}\,"1"} - (k' \times \mathrm{yr})$$

where $\mathrm{BSi}_{\mathrm{pre}\ "i"}$ is the biogenic silica remaining undissolved within the sediment in year "i" of the burial process, $\mathrm{BSi}_{\mathrm{pre}\ "1"}$ is the biogenic silica empirically measured at the superficial layer of sediment in the core (i.e., at year 1) of the *Vazella* ground, k' is the dissolution rate constant (i.e., 1—the BSi preservation rate constant), and *yr is* the age of the corresponding sediment depth expressed in years (see Data File S1).

We calculated first the dissolution rate constant (k') of the *V. pourtalesii* biogenic silica by determining empirically the loss of biogenic silica mass between the upper sediment layer and that at 12.5 cm, which was assumed to contain the same biogenic silica mass that at 23 cm, after considering a constant deposition rate of biogenic silica and negligible dissolution below 12.5 cm. For the calculations, the biogenic silica mass was scaled to a sediment thickness equivalent to 1 yr of sediment deposition (applying the average rate of sediment deposition), then scaled to m^2 (applying the sediment density). We also assumed k' to be similar at all sediment depth above the biogenic silica dissolution threshold (12.5 cm), as k' for other biogenic silica types is known to change minimally above the preservation threshold (Sarmiento and Gruber 2006). Below 12.5 cm, k' became zero, as corresponding to a situation of negligible dissolution.

By using the described equation, the sponge biogenic silica dissolved as silicic acid and that remaining as particulate biogenic silica for each successive annual sediment layer during the burial process was calculated (Data File S1). The accumulated stocks of both preserved sponge biogenic silica and sponge biogenic silica dissolved as silicic acid in the pore water of the 23 cm sediment column were obtained by summing all the annual values over the number years (i.e., 767 yr) needed to build the 23-cm sediment column (Data File S1). These biogenic silica and silicic acid stocks in the sediment, which stand for a sediment column of 23 cm in height and m^2 in area within the sponge closure, were subsequently extrapolated across the cells of presence probability in the sponge ground extent.

The rate at which the silicic acid freed to the pore water from the buried sponge biogenic silica is subsequently diffusing to the bottom water across the sediment–water interface to become available again to silicifiers is hard to be calculated. Unfortunately, inclement weather at sea prevented us to incubate sediments and measure in situ silicic acid efflux rates. To palliate the loss of our empirical approach to this parameter, we used the average silicic acid efflux measured in a previous study (Andrews and Hargrave 1984). The study was conducted from March to May in three consecutive years during the 1970s, focusing on sediments from the Emerald Basin (Stas. 1–4; Fig. 1C). It involved four study stations (Fig. 1C), one for in situ determination of the silicic acid efflux using a sediment incubation chamber; the three other stations provided sediment cores for estimating silicic acid efflux rates in the laboratory from pore-water silicic acid concentrations. All four stations were located in the vicinity of—but outside—the sponge grounds, ranging in distance between ~ 5 and 16 km east from the limit of the Sambro Bank Sponge Conservation Area (Fig. 1C). The presence probability model for *V. pourtalesii* on the entire Scotian Shelf (Beazley et al. 2018) indicates that those three stations were located in areas of moderate sponge presence probability (Sta. 1 = 0.458, 2 = 0.354, 3 = 0.374). From this basis, the average efflux (0.90 ± 0.40 mol Si m^{-2} yr^{-1}, n = 10) obtained from Andrews and Hargrave's data (1984) was weighted across the probability bins over the extension of the sponge grounds. However, given that Stas. 1–3 are located within Emerald Basin's Main Basin slighter deeper than the main sponge grounds, its sediments could well have accumulated spicules transported or suspended from the densest areas of the shallower adjacent sponge ground. Accumulations of dead individuals of *V. pourtalesii* have been seen in ROVs surveys in Emerald Basin, that appear to be individuals dumped by trawl vessels

and that pool in one area from currents. Such processes may cause the sediments outside the sponge ground to have a sponge spicule content higher than strictly corresponding to the predicted probability of sponge presence. If this effect is not accounted for, the extrapolation into the sponge ground of the silicic acid efflux rates measured for sediments outside will cause an overestimation of the silicic acid efflux within the sponge ground. Therefore, to conduct a more conservative approach, we considered that the average silicic acid efflux obtained from Andrews and Hargrave's data (1984) does not correspond to a sponge presence probability of 0.35–0.46, but rather to a probability of 0.575, which may better reflect the input of spicules dispersed from the adjacent sponge grounds, complementing the spicules deposited from the sponges living at the coring sites. Of note, the unavailability of empirical data other than those obtained by Andrews and Hargrave (1984)—hourly silicic acid efflux rates derived from 24 h incubations conducted only from March to May months—forced us to extrapolate their time-constrained figures to a complete year period. Therefore, our calculations may not incorporate adequately the real annual variability in the silicic acid efflux from the sediment.

To document visually whether the dissolution of the sponge spicules buried in the sediments was contributing to the silicic acid efflux from the sponge ground, we examined the stage of attrition of the spicules using a high resolution Jeol Field Emission J1700S Scanning Electron Microscope. Comparative observations were conducted on spicules collected by pincers from living individuals, spicules deposited at the superficial sediment layer (0 cm), and spicules buried at 23 cm. To facilitate relevant comparisons, spicules were dried at 60°C for 2 d and carbon-coated prior to microscope examination, and were not subjected to cleaning or rinsing in distilled water or acidic solution.

Basic hydrography of bottom water

To learn how the silicic acid efflux from the sediment at the sponge grounds could disperse, we aimed to characterize the basic hydrography of the bottom water at the sponge grounds. Hydrography was characterized by an Aquadopp 2000 kHz current meter (Nortek™) attached to a NIOZ designed ALBEX lander which was deployed inside the Sambro Bank Sponge Conservation Area (43.07694°N, 63.07694°W) at a depth of 155 m (further details in Beazley et al. 2017). The logger was positioned at 2 m above the seafloor and sampled at an interval of 900 s from the 7 September 2017 to the 22 June 2018, collecting data in 20 bins of 0.5 m. Current velocity and direction data recorded at 3 m above the bottom were analyzed and plotted using R software.

Closing the Si cycle at the sponge ground

The quantified flux rates and stocks—obtained as explained in the previous "Methods" sections—were used to summarize the Si cycle across the system of the sponge grounds (i.e., those areas predicted with > 70% presence probability) in relation with the various biogeochemical processes identified. The integration of the cycle is progressively presented and discussed throughout the "Discussion" section.

Results

Sponge morphometry and allometries

The morphometric parameters (Table 1) of the 34 collected individuals showed a variety of robust and statistically significant, pairwise, linear and non-linear relationships. Here we summarize those that were of interest to derive the volume of the sponges from the digital images and video frame grabs collected in the Sambro Bank Sponge Conservation Area.

The maximum width of the sponges, which is often attained at a sub-distal position (Fig. S1), was linearly related to sponge height (Fig. 3A). However, when the two smallest individuals (< 2 cm in height) of the collection were discarded, the relationship became sigmoidal (Fig. 3B), suggesting that the sponges grow faster in width than in height once a certain height is attained after settlement. Interestingly, the thickness of the body wall at the atrium—a parameter which is hard to estimate from images or video—was non-linearly related to the maximum width and height of the sponges (Fig. 3C,D). Such significant, strong relationships were often used to estimate wall thickness when calculating the volume of the sponges through the truncate-cone approach (see section "Methods"). Both maximum width and total height of the sponge body were also significantly related to volume (Fig. 3E). For these two regressions, we set the shared constraint that the maximum body volume in the population is approximately 15,000 mL, following measurements obtained from the digital images and video frame grabs. Importantly, when the volume of the collected sponges was estimated from its significant relationships with the maximum width or total length of the sponge body (Fig. 3E), the standard error of the prediction (vs. volume values obtained by water displacement) was only ± 57 mL. Likewise, when the volume measured by water displacement was compared with that estimated through the truncate cone approach (Fig. 3F), the prediction error was only 8.4 ± 5.4% of the measured volume.

Physiological and skeletal conversions were also possible because a strong linear relationship between the volume and the dry weight of the individuals was found (Fig. 3G), as well as between the dry weight and the biogenic silica content (Fig. 3H). Additionally, it was also possible to reliably estimate the biogenic silica (BSi) content (g) of the sponges from its linear relationship (not shown in graphs) to volume (in mL), following the equation "BSi= 0.271 + 0.057 volume" (n = 22, R^2 = 0.843, $p < 0.001$, SE Estimate = 2.9 g BSi), which was derived from 22 collected sponges that were processed for biogenic silica content by either ashing in furnace or desilicification in hydrofluoric acid (Table 1). This species can be considered as highly silicified, since the silica skeleton

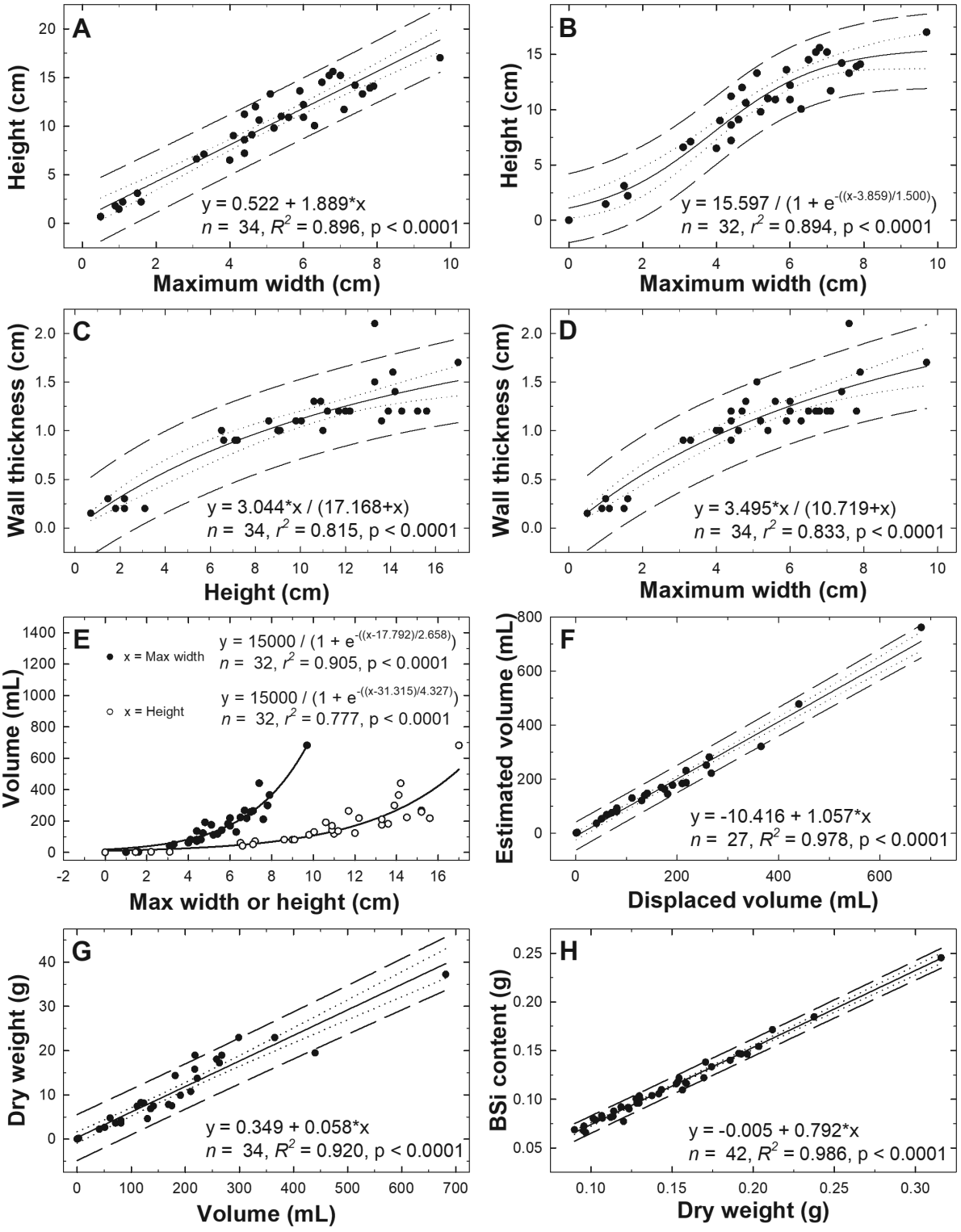

Fig 3. Summary of relevant relationships between pair of morphometric parameters, which in all cases were strong and with statistical significance. Note that the maximum width of the sponges was linearly related to sponge height (**A**). However, when the two smallest individuals (< 2 cm in height) of the data set were discarded, the relationship became sigmoidal (**B**), suggesting that the sponges grow faster in width than in height once a certain height is attained after settlement.

represents 84.1% ± 12.8% of the body dry weight (n = 22) and consists of 55 ± 17 mg of biogenic silica per mL of body volume in living individuals.

Collectively, the results indicate that the volume of sponges and their biogenic silica content can reliably be estimated through a variety of approaches, and that selecting for one or another will depend on the availability of the linear morphometric parameters that can be retrieved from digital images or video frame grabs.

Sponge standing crop and biogenic silica stock

In the assessment of sponge density through the 1 × 1 m quadrat approach, sponges occurred in 29 out of the 32 quadrats, corroborating Beazley et al.'s assumption (2018) that presence probability in the closures reaches its maximum (i.e., > 0.9). Sponges totaled 121 individuals in the 32 quadrats, ranging from 0 to 12 ind. m^{-2}, with an average density of 3.78 ± 3.22 ind. m^{-2}. Note that the error associated to the mean values is large not because a defective approach but because some m^2 quadrats were empty of sponges and others contained high numbers. The video-transect approach captured a total of 1646 sponge individuals, with an average density of 3.52 ind. m^{-2} (associated error unavailable), similar to the value rendered by the quadrat approach. In the quadrat approach, body size ranged from 2.2 mL to 4.9 liter (Fig. 4A), while it ranged 4.8 mL to 10.7 liter (Fig. 4B) in the transect approach. Both approximations indicated that most individuals were < 200 mL (Fig. 4), reflecting high juvenile abundance in a demographically healthy population. From the sets of ROV observations, we can hypothesize that maximum height in the population is about 40 cm and maximum volume about 15 liter. For further extrapolations, we preferred to use the average density of 3.8 ± 3.2 ind. m^{-2} empirically measured within the Sambro Bank Sponge Conservation Area through the quadrat approach rather than the density of 3.52 ind. m^{-2} produced by the transect approach, because the latter does not carry an associated error and hinders error propagation. When average density was weighed across the cells of presence probability and extrapolated over the area of the sponge ground (Data File S2), some 6479 ± 5518 million sponges were estimated to live at the 2104.6 km^2 aggregation.

The average biomass per m^2 was 1.6 ± 2.8 liter in the quadrat approach and 1.81 liter (associated error unavailable) in the transect approach. When the former value was used for extrapolation across the presence probability cells, a global standing stock of 2790.6 ± 3832.3 million liter of sponges was attained. The highest sponge biomass was distributed in two core areas (Fig. 5).

When the linear relationship between sponge volume and biogenic silica content was applied to each of the 121 sponges found in the 32 quadrats at Sambro Bank Conservation Area, a Si content of 43.8 ± 74.6 g m^{-2} in the form of skeletal biogenic silica resulted. When this average was weighted across the presence probability cells and then extrapolated across the extension of the sponge ground, a Si stock of 2674 ± 3653 × 10^6 mol Si (75.1 ± 102.6 million kg Si) was revealed within the skeletons of the living population.

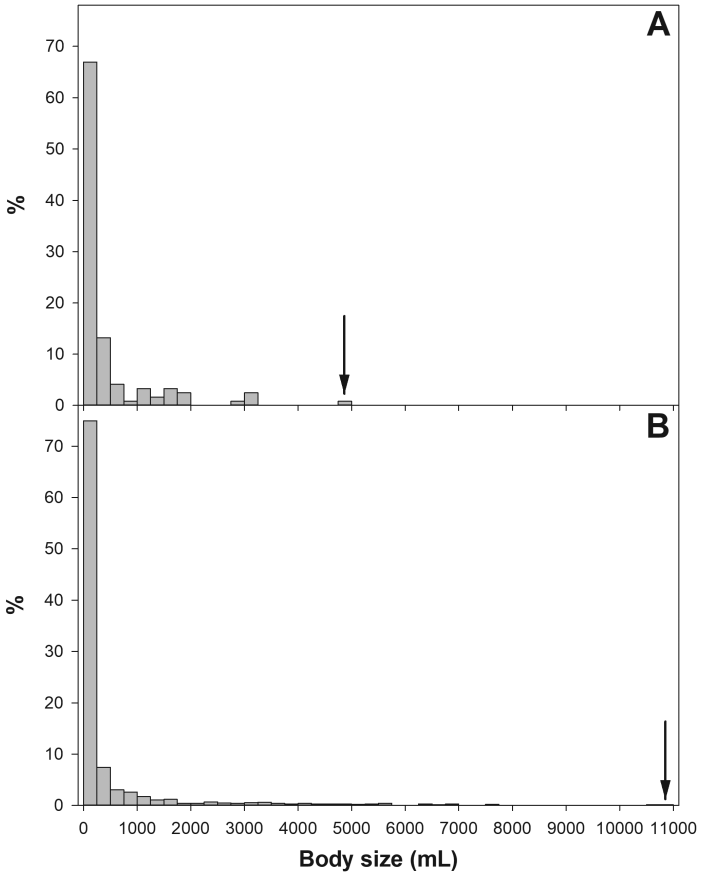

Fig 4. Body size distribution in the *V. pourtalesii* population measured at Sambro Bank Conservation Area through the quadrat (**A**) and video transect (**B**) approaches. Arrows indicate the largest individual volume found in each approach.

Temporal and spatial availability of silicic acid

By selecting the monthly averaged silicic acid concentrations and their corresponding monthly maximum and minimum records from a decadal deep-water sampling on the central Scotian Shelf published by Petrie et al. (1999), a global (n = 60) mean silicic acid concentration of 16.9 ± 8.7 μM was obtained. A similar silicic acid concentration of 15. 6 ± 0.7 μM was found from five seawater samples collected from 10 to 20 cm above the bottom in the densest area of the sponge aggregation at Sambro Bank Sponge Conservation Area collected through ROPOS.

Interpolated silicic acid concentrations in the bottom-water layer and at mid-depths across the Scotian Shelf are shown in Figs. 6, 7. The spatial distribution of the original data sets that supported the interpolations and that of the interpolation errors are given in Figs. S2, S3. The interpolations revealed a

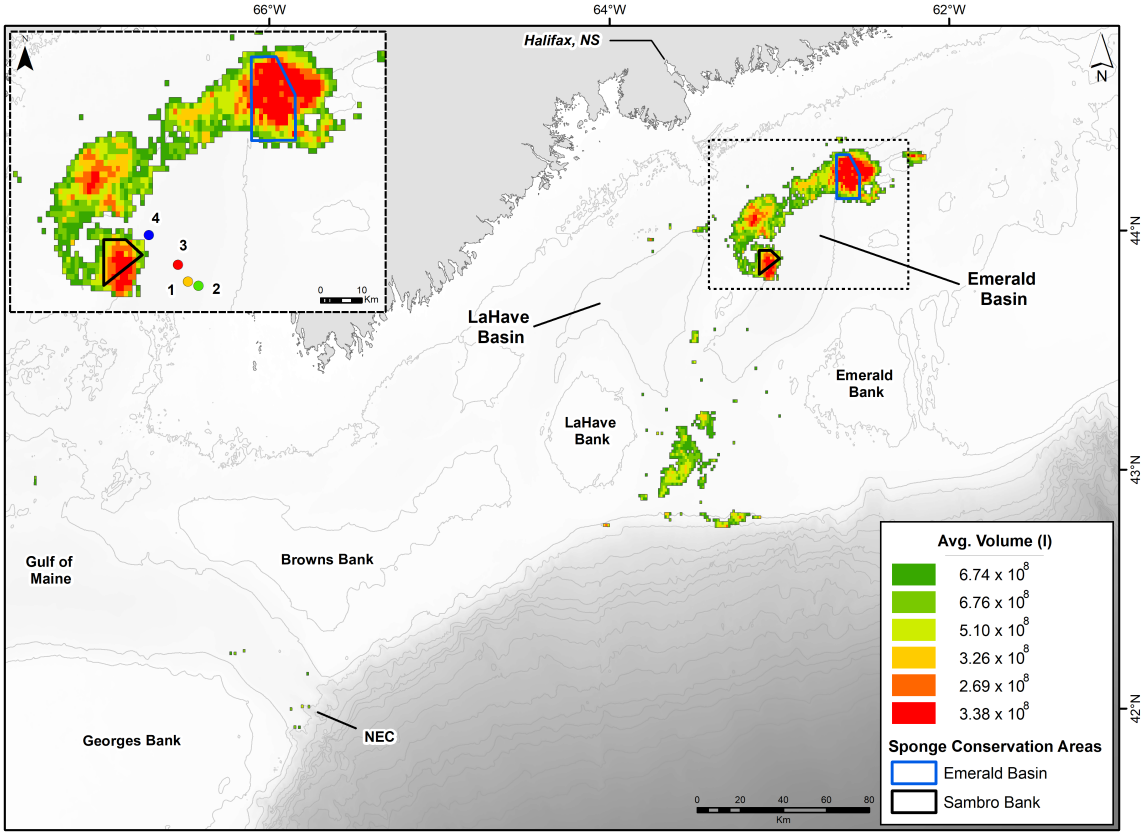

Fig 5. Average volume (liters) of *V. pourtalesii* across the sponge grounds, that is, in those areas predicted with > 70% presence probability from Beazley (2018). Volume was calculated for those 1 × 1 km grid cells with presence probability values binned into 5% intervals (e.g., > 70–75%, > 75–80%, etc.). Stations 1–4 show the location of the sites selected by Andrews and Hargrave (1984) to determine silicic acid concentrations in pore water and silicic acid efflux from the sediments to the bottom water (see Fig. 1C).

general scenario in which, irrespective of season, two large patches of comparatively high silicic acid concentrations in bottom water occur adjacent to each of the two sponge high-density areas in the *Vazella* grounds. The *Vazella* grounds (> 70% presence probability areas) experienced a range in summer bottom silicic acid from 8.0 to 22.6 μM (average 15.6 ± 3.7 μM) and winter silicic acid from 9.0 to 16.2 μM (average 12.3 ± 0.9 μM). Slightly higher silicic acid concentrations were found just outside of the sponge grounds, in a patch to the east of Emerald Basin and in LaHave Basin (Fig. 6A,B), where values reached up to 25.9 μM in the summer. Silicic acid at mid-depths in the *Vazella* sponge grounds was lower than that at the bottom in the same season, ranging from 1.8 to 17.0 μM (average 7.5 ± 3.2 μM) and 1.9 to 10.4 μM (average 6.3 ± 1.9 μM) in summer and winter, respectively. More importantly, the high-silicic acid patches found in bottom water adjacent to the most populated areas of the sponge grounds did not occur in mid water.

Overall, silicic acid in the bottom layer ranged from > 0 to 39 μM and > 0 to 29 μM for summer and winter, respectively. Although the number of silicic acid samples available over the more densely populated areas of the sponge ground is lower than in other areas of the central Scotian Shelf (Fig. S2A,C), the silicic acid surfaces resulting from the interpolation were considered statistically reliable, since reasonable errors (of only up to 1.4 μM Si) characterized interpolations for silicic acid of bottom water in both summer and winter (Fig. S2B,D). Yet, the low number of data collected directly over the *Vazella* grounds in the winter season (Fig. S2A,C) suggest interpolations for winter values to be interpreted with caution. Limited availability of data points and higher inter-annual variability in some regions of the study area resulted in the highest errors, but those areas did not involve the sponge grounds, as they are located particularly along the slope and in the Laurentian Channel at the edge of the eastern Scotian Shelf. A comparison of our interpolated surfaces with those of Petrie et al. (1999) revealed similar silicic acid-rich patches in summer and winter bottom water at locations equivalent to those in our data. These silicic acid pockets either disappear or become much weaker at shallower depths (50 m) in the water column. The agreement in the two data series of such a spatial–temporal

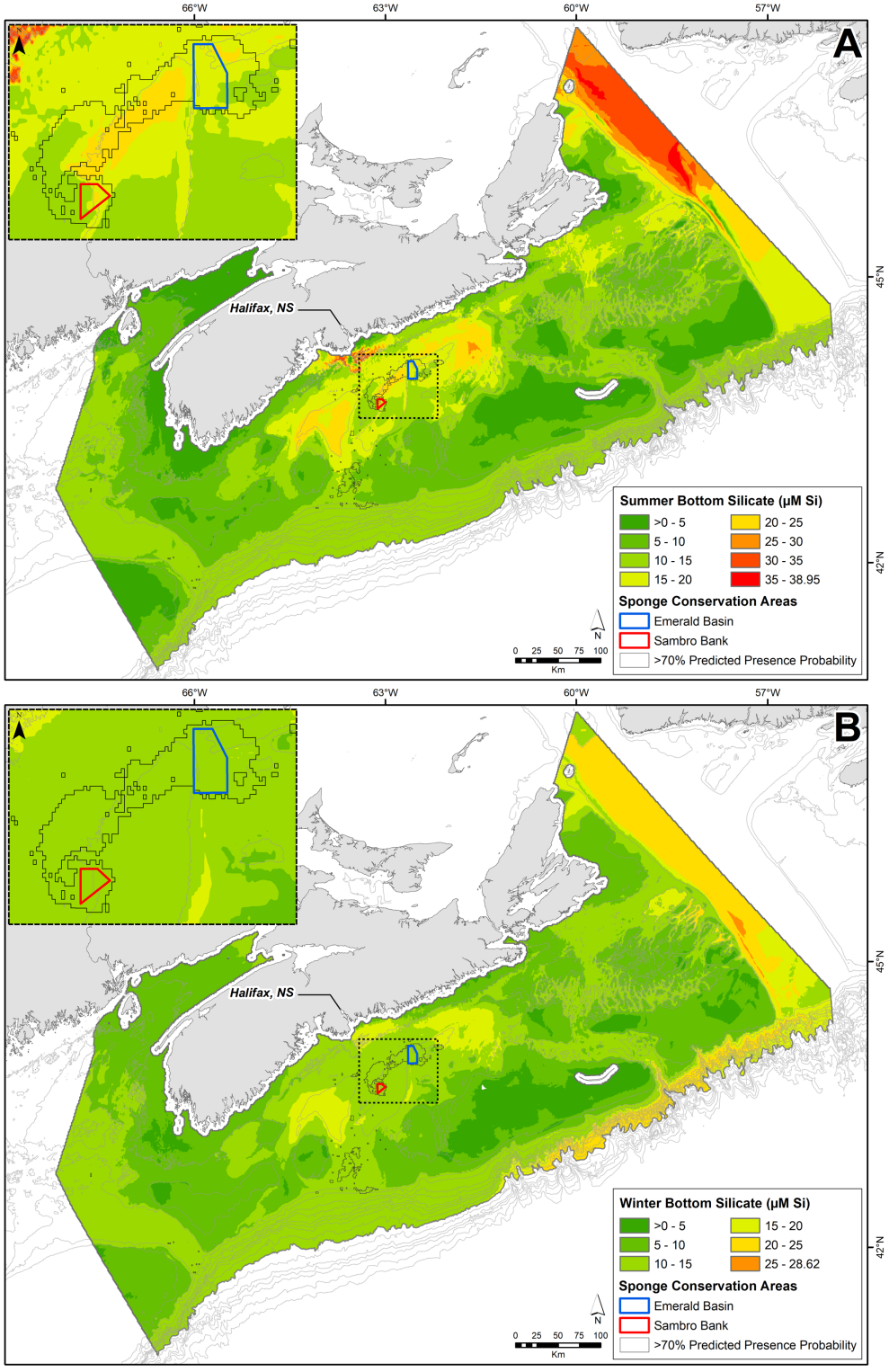

Fig 6. Summer (**A**) and winter (**B**) optimally estimated silicic acid (silicate) concentration (μM Si) in the bottom layer (within 6 m from the seabed) across Fisheries and Oceans Canada's Maritimes Region, to 2000 m depth. The inset on the left corner details concentrations around the sponge closures.

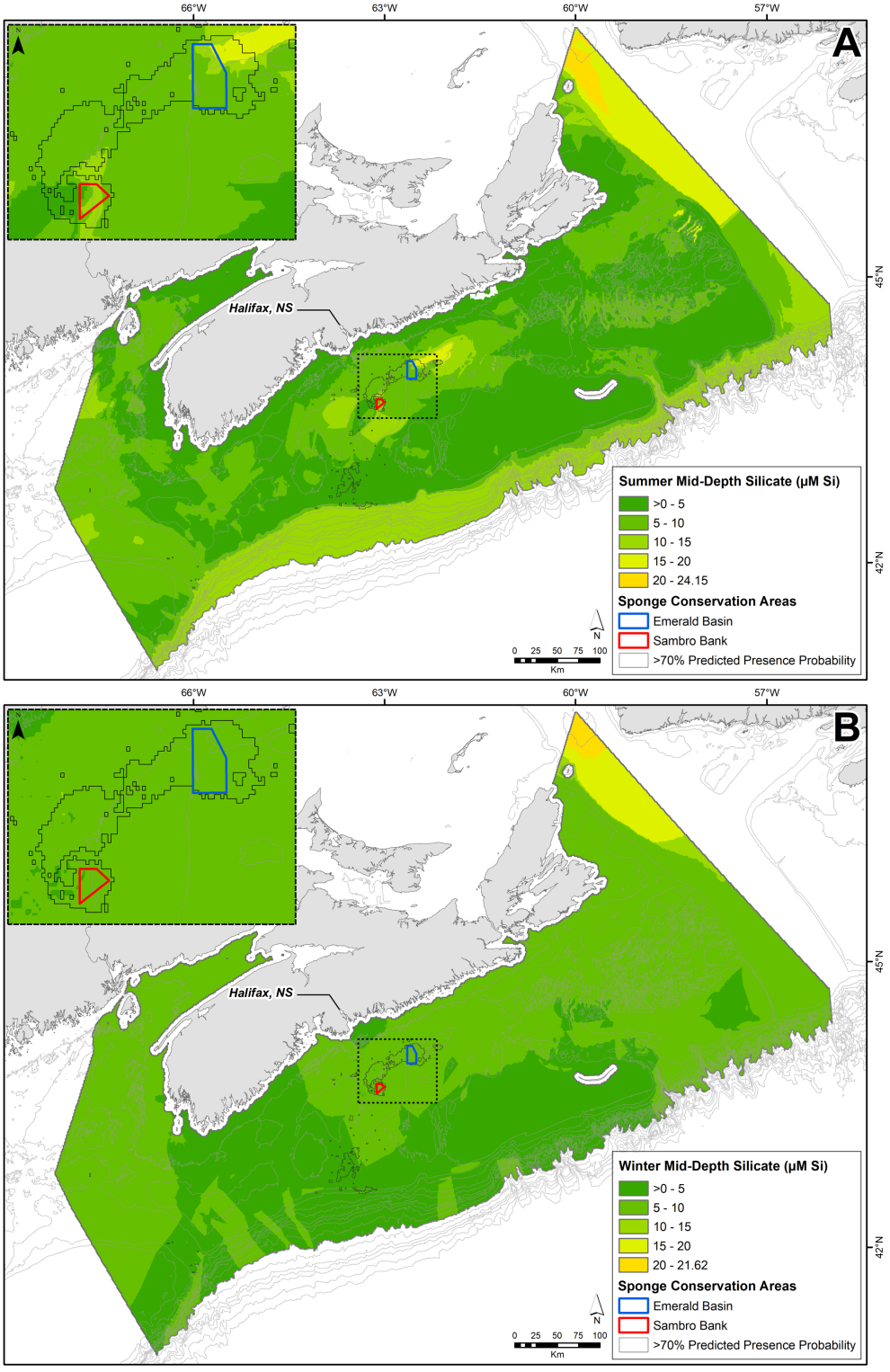

Fig 7. Summer (**A**) and winter (**B**) optimally estimated silicic acid (silicate) concentration (μM Si) at mid-depths (50% $\pm$ 5% of total water depth) across Fisheries and Oceans Canada's Maritimes region, to 2000 m depth. The inset on the left corner details concentrations around the sponge closures.

pattern suggests that the pockets of silicic acid-enriched bottom water do occur. Likewise, their absence or lower extension and intensity at intermediate depths in the water column suggest that the silicic acid source is at the bottom rather than at the ocean surface.

Silicic acid consumption by live sponges

Silicic acid consumption was estimated by two different approaches. First, the kinetic equation describing the rate of silicic acid utilization (μmol of Si mL^{-1} sponge h^{-1}) by *V. pourtalesii* as a function of sponge biomass (in volume) and environmental silicic acid availability was applied to the intersections between the cells of sponge biomass (Fig. 5) and those of silicic acid concentration in bottom water for both summer and winter (Fig. 6A,B), yielding an annual silicic acid utilization of $610 \pm 838 \times 10^6$ mol Si yr^{-1} (Data File S2). In the second approach, the kinetic equation was applied to the biomass in the quadrats at Sambro Bank Sponge Conservation Area, after considering that the annual silicic acid availability to the sponges can be summarized by the decadal silicic acid average of 16.93 μM obtained from Petrie et al. (1999). By this assumption, a mean silicic acid consumption of 11.7 ± 20.0 g Si m^{-2} yr^{-1} was obtained from across the two closure areas, which was subsequently weighed across the cells of presence probability and extrapolated across the sponge ground. The approach yielded a consumption of $713 \pm 980 \times 10^6$ mol Si yr^{-1} (Data File S2). By combining the result of approaches 1 and 2, an average silicic acid consumption of $662 \pm 818 \times 10^6$ mol Si yr^{-1} was obtained. Note that the large errors associated to the average consumption rate do not derived from poorly constrained estimates of either the silicic acid availability to the sponges or the kinetics of silicic acid consumption by this species. Rather, it derives from the large variability associated to the spatial distribution of the sponge biomass per m^2, which ranged from empty quadrats to quadrats containing up to 12 individuals.

The estimated average consumption rate involves a substantial annual removal of silicic acid from the bottom seawater around the sponge grounds. At first sight, such a silicic acid removal by the living sponges would come into apparent conflict with the results of the above section suggesting occurrence of a silicic acid source at the seafloor around the sponge aggregations. However, the investigation of the post-mortem biogenic silica processes in the sediment provides an explanation.

Sponge biogenic silica in sediments: Dissolution, preservation, and reservoirs

The light microscopy study of the sediments from Sambro Bank Sponge Conservation Area revealed a content of sponge biogenic silica of 0.334 ± 0.026 mg Si per g of sediment at the superficial layer and 0.117 ± 0.038 mg Si per g of sediment at a burial depth of 23 cm. The wet bulk density of the sediment was estimated at 1.652 g cm^{-3}. A local sediment deposition rate of 0.3 ± 0.0 mm yr^{-1} indicated that the age of the sediment at 23 cm was about 767 years old (Data File S1). Likewise, the age of the sediment at 12.5 cm, where sponge biogenic silica preservation starts, was estimated at 417 years old. From the above parameters, the content sponge biogenic silica in the sediment thickness corresponding to the most recent year of deposition (year 0) and to year 767 were scaled at m^2, resulting respectively in 165.6 ± 12.9 and 57.9 ± 18.79 mg Si m^{-2} yr^{-1}. When the former amount was weighted across the presence probability cells and extrapolated over the sponge ground, it resulted in a global deposition rate of $10.1 \pm 0.8 \times 10^6$ mol Si yr^{-1} in the form of sponge silica (Data File S1).

The difference in sponge biogenic silica content between the sediment layers corresponding to year 0 and year 417 (where biogenic silica preservation is assumed to start) allowed estimating the annual dissolution of sponge biogenic silica at $0.156\% \pm 0.024\%$ (i.e., $k' = 1.556 \times 10^{-3}$), which in the studied corer translated into an annual loss in the buried biogenic silica mass of *V. pourtalesii* of 0.258 ± 0.047 mg Si m^{-2} yr^{-1} (Data File S1). When these annual calculations were projected over the 767 years of the 23 cm-thick sediment column, the reservoirs of biogenic silica that remains buried (66.8 ± 9.3 g Si m^{-2} yr^{-1}) and that has been freed as silicic acid (60.1 ± 9.0 g Si m^{-2} yr^{-1}) to the pore water were obtained per m^2 of sponge closure (Data File S2). When these values were extrapolated over the density cells of the sponge grounds, it was calculated that a biogenic silica reservoir of $4074 \pm 566 \times 10^6$ mol Si is currently accumulated in the 23 cm thick sediment column over the extension of the grounds (Fig. 8) and that, through the progressive dissolution of part of the buried sponge biogenic silica during that same period, about $3673 \pm 553 \times 10^6$ mol Si have been freed to the interstitial water across the extension of the sponge grounds (Data File S2). The ratio between the biogenic silica definitively preserved below 12.5 cm in the sediment and that dissolved as pore-water silicic acid indicates that, in the case of *V. pourtalesii*, the biogenic silica preservation is $35.1\% \pm 10.1\%$, a figure lower than the average ($45.2\% \pm 27.4\%$) known for sponge biogenic silica (Maldonado et al. 2019). The preservation value translated into a rate of permanent sponge biogenic silica burial of $3.5 \pm 0.90 \times 10^6$ mol Si yr^{-1} through the *Vazella* grounds (Data File S2). While the fate of the particulate biogenic silica reservoir built in the sediment was relatively easy to trace, to elucidate the fate of the silicic acid freed from the buried biogenic silica to the pore water proved far more complicated.

The silicic acid annually dissolved from the deposited and buried spicules slowly diffuses from the interstitial water towards the bottom water through the sediment surface. As inclement weather during the 2017 cruise prevented us from conducting in situ sediment incubations, estimates of the silicic acid efflux from the sediment of the sponge grounds were based on efflux rates previously measured by Andrews and Hargrave (1984) at Emerald Basin (Fig. 1C). When the

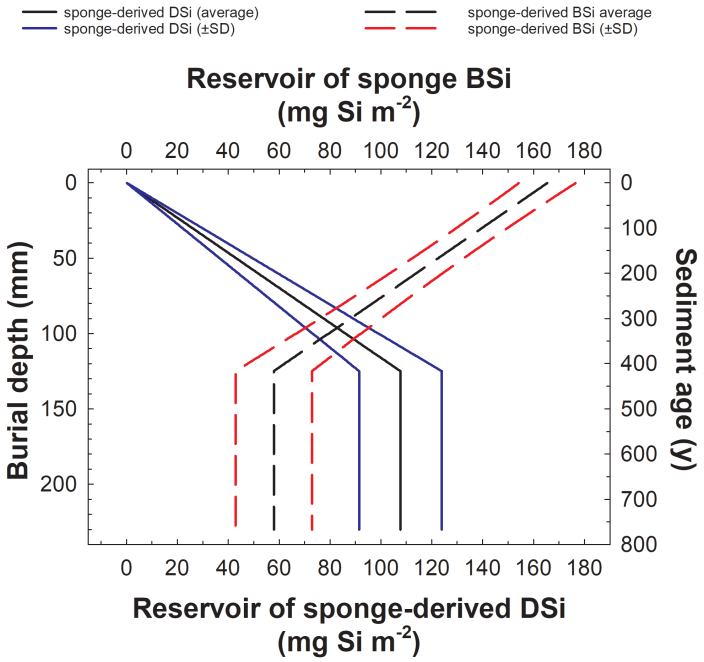

Fig 8. Estimated annual decrease of the sponge biogenic silica (BSi) reservoir during its burial in the 23 cm-thick sediment column as consequence of its progressive partial dissolution as silicic acid (DSi) in the pore water, following the equation "$BSi_{pre\ "i"} = BSi_{pre\ "1"} - (k' \times yr)$." $BSi_{pre\ "i"}$ is the BSi remaining undissolved at year "*i*," $BSi_{pre\ "1"}$ is the BSi empirically measured (165.57 ± 12.88 mg Si m^{-2}) during the first year of deposition at the sediment surface, k' is the dissolution rate constant (estimated at $1.556 \pm 0.242 \times 10^{-3}$) above the preservation threshold in the sediment (12.5 cm), and *yr* the age of sediment expressed in years (see Data file S1). Sediment age at 12.5 and 23 cm was estimated at 417 and 767 years respectively, from an average sediment deposition rate of 0.3 ± 0.0 mm yr^{-1}. Note that BSi preserved at year 417 ($BSi_{pre\ "417"}$) and in subsequent years renders exactly the same average value of the sponge BSi content (57.88 ± 18.69 mg Si m^{-2}), which is that empirically determined at a burial depth of 23 cm (767 years old). The ratio between the sponge BSi preserved and that dissolved below 12.5 cm in the sediment indicates the preservation (35.1% ± 10.1%) vs. the dissolution (64.9% ± 10.1%) potential of the *V. pourtalesii* BSi.

average efflux rate obtained from literature data (i.e., 0.9 ± 0.4 mol Si m^{-2} yr^{-1} for a presence probability cell of 0.575) was weighted across the presence probability cells and extrapolated across the extension of the sponge grounds, an annual silicic acid efflux of $2684 \pm 1199 \times 10^6$ mol Si yr^{-1} was obtained (Data File S2).

To visually examine the process of sponge biogenic silica dissolution during burial, the attrition levels of spicules buried in 23 cm of sediment, of spicules collected from the superficial sediment, and of spicules protruding from the surface of living sponges were comparatively documented by scanning electron microscopy (Figs. 9, 10). The approach revealed that the reason why the preservation of the biogenic silica of *V. pourtalesii* is lower than that reported for other sponges is likely that its larger spicule types experience a rapid delamination of the silica layers. The skeleton of *V. pourtalesii* consists of 10 distinct morphological types of spicules. As a microscopic description of all types is beyond the scope of this study, we focused on the two largest types (pentactines and monaxons), both of which protrude beyond the dermal surface of the sponges (Fig. 9A–C). Pentactines have one ray inserted in the sponge body and the four others arranged in a plane orthogonal to the former ray and located outside the sponge, as a sort of umbrella over the sponge surface (Fig. 9B–D). The rays of the pentactines are spiny (Fig. 9E–G) and can be up to 1.4 cm long. Monaxons are needle-like spicules that can be up to 5.4 cm in length, with a smooth (non-spiny) surface (Fig. 9H). The combination of both types of protruding spicules is likely a mechanism of defense against generalist predators, but it also prevents from settlement of fouling invertebrates and settling of sediment directly on the filtering epithelium of the sponges.

The microscope inspection revealed that these spicules are formed by concentric layers of silica that, unlike in most other sponge spicules, are not continuous over the spicule length (Fig. 9G,H). While this patchy silicification pattern is not always obvious for the spicules that are still embedded in the body of the living sponges (but see Fig. 9F,G), the limits of adjacent silica patches become very evident in the spicules that are deposited in the sediments (Fig. 10). The borders between patches appear to act as points that facilitate a rapid silica dissolution, so that large pieces of the external silica bark loosen and start detaching from the rest of the spicule axis (Fig. 10A–G). The progressive delamination process drastically increases the specific surface area exposed to seawater for the dissolution of the silica that initially made each spicule and it also contributes to a rapid disappearance of the large spicules, as unitary entities, from the sediments during the burial process. The idea of a rapid spicule fragmentation and dissolution is also consistent with the results from a comparison of size distribution of the spicule remnants retrieved in 30 mg of dry sediment (Fig. 11). It reveals that the number of large spicules (i.e., those larger than 10^5 μm^3 in volume) decreases by half during the burial process, from 124 in the superficial sediment to only 69 at 23 cm (Fig. 11). More importantly, the volume reached by the skeletal remains in the superficial sediments is about three orders of magnitude higher than at 23 cm (Fig. 11). The microscope inspection made clear that "silica barks" resulting from delamination were the only siliceous remnants that occurred abundantly in the sediments at 23 cm (Fig. 10I). The microscleres (Fig. 9I), abundant in the skeleton of the living sponges, also appear to be dissolved rapidly after deposition. A total of 162 identifiable microscleres (7.1%) were identified out of the 2293 spicules or spicules fragments found in the superficial sediments, whereas only 1 was found out of 863 pieces (i.e., 0.1%) retrieved at 23 cm. The few spicule remnants identified at 23 cm characteristically showed their silica surface entirely covered with dissolution scars (Fig. 10J–M), a feature that was not seen in the spicules of the superficial sediment. Some of these spicule remnants at 23 cm also showed axial

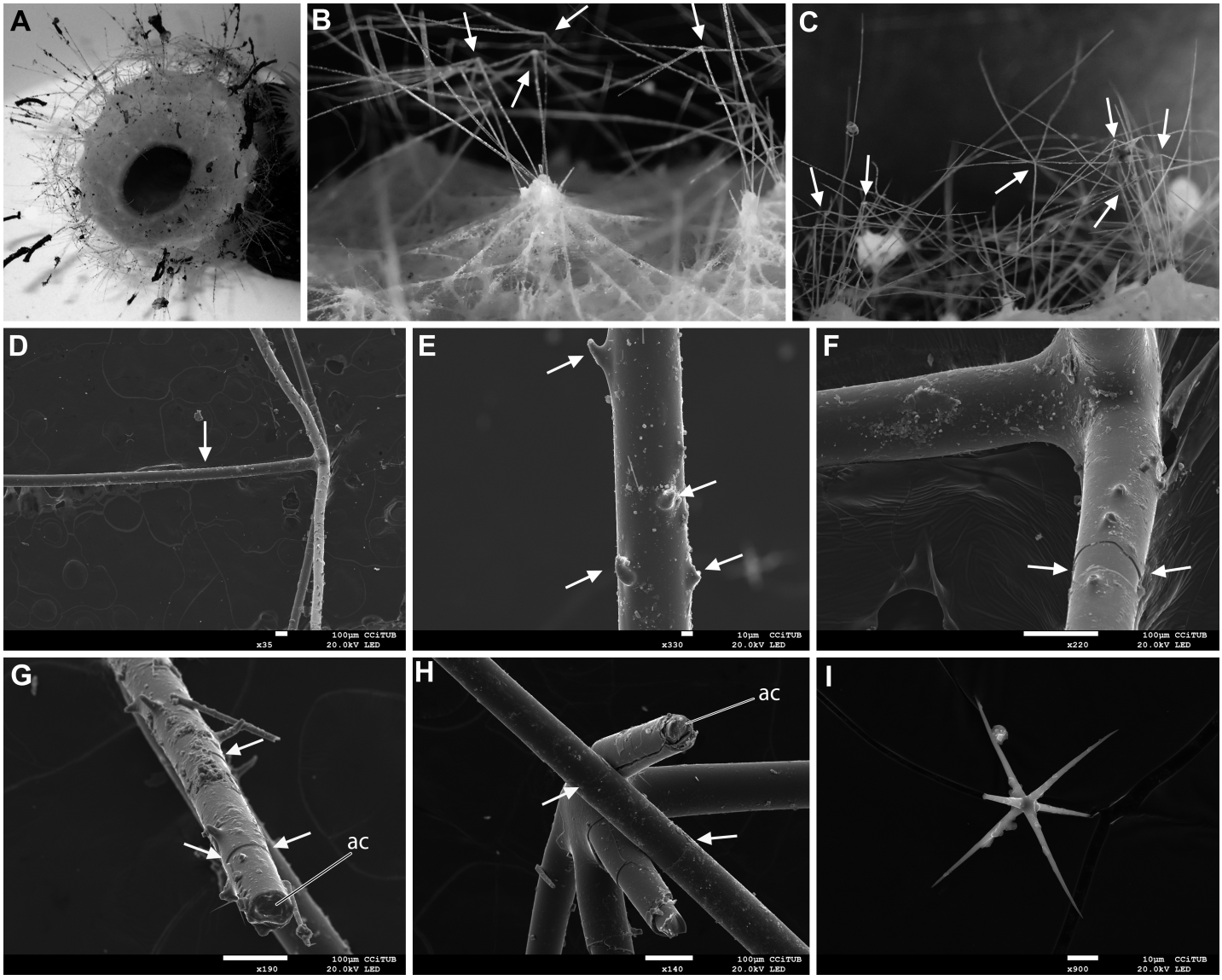

Fig 9. Features of the spicules in living *V. pourtalesii*. (**A**) Top view of an individual of *V. pourtalesii*, showing the large osculum and the abundance of large protruding spicules around the body. (**B** and **C**) Details of the sponge surface indicating by arrows the most obvious protruding pentactinal spicules. (**D**) General view of a pentactine extracted by pincers from the body surface, showing the ray that was inserted into the body (arrow) and the four orthogonal rays. (**E**) Detail of the surface of a pentactine, showing large spines (arrows). (**F**–**G**) Detail of the surface of a pentactine, showing that the most external silica layers is not continuous. Obvious discontinuities in the silica layers are indicated by arrows. (**H**) Monaxonic protruding spicule on top of a pentactine, showing subtle borders (arrows) between adjacent siliceous patches, providing evidence of a non-continuous silica layer. Note also that the pre-existing axial canal ("ac" in G and in H) is not visible because within the rays, because it has been obliterated by secondary silica deposition. (**I**) Microsclere in the form of hexactinous oxyhexaster.

canals that had started dissolving (Fig. 10N). This was another feature found neither in the spicules of the living sponges nor in those of the superficial sediments, which consistently showed the axial canal obliterated by silica (Figs. 9G,H, 10H).

Collectively, the results of the electron microscopy study and the analyses of spicule abundance and size in the sediment support the notion that the siliceous spicules of *V. pourtalesii* get fragmented and dissolved more rapidly than previously demonstrated for most other siliceous sponges (see "Discussion" section).

Basic hydrography of bottom water

The current meter recorded the direction and amplitude of near bottom currents at the *Vazella* ground in the Sambro Bank Sponge Conservation Area, registering a net southward flow during the 10-month deployment. The average near

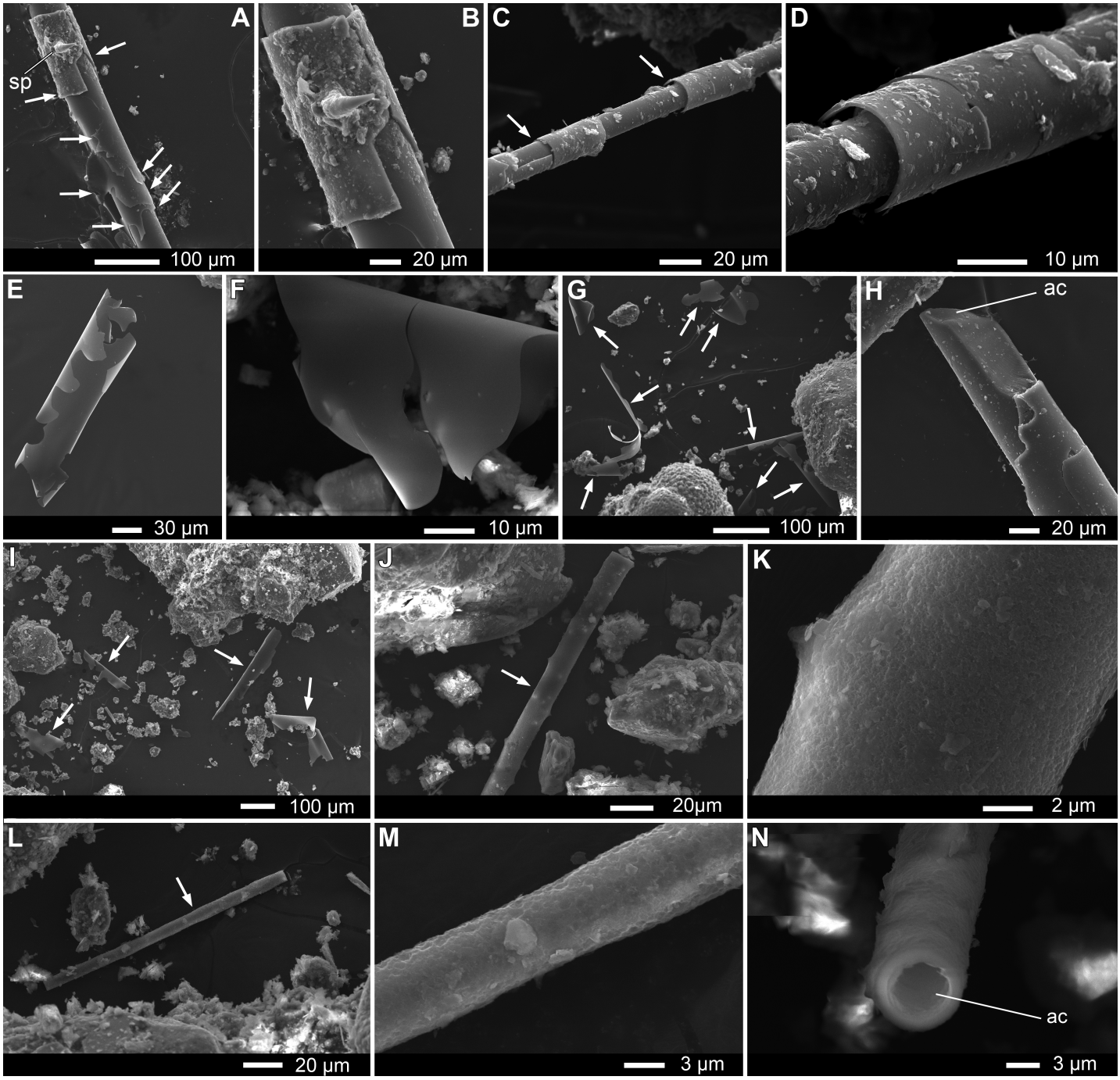

Fig 10. Features of *V. pourtalesii* spicules once being deposited to the sediments. (**A** and **B**) Details of the remnants of a spiny ray of a pentactine at the superficial sediment, showing the intense process of silica delamination, by which spines (sp.) are lost first and subsequently the underlying silica layers (arrows). (**C** and **D**) Details of the intense silica delamination (arrows) in a monaxonic spicule at the superficial sediment. (**E** and **F**) Silica "barks" detached from the sponge spicules. (**G**) Abundance of detached silica barks (arrows) among the grains of the superficial sediments. (**H**) All examined spicules from the superficial sediment showed axial canals (ac) secondarily obliterated by silica deposition. (**I**) At 23 cm in the sediments, large spicule fragments (> 500 μm) were completely absent, being replaced by abundance of detached silica barks (arrows). (**J–M**) At 23 cm in the sediments, recognizable spicule fragments were scarce and typically shorter than 200 μm (**J** and **L**), showing their external silica surface with marked scars of dissolution (**K** and **M**), which were never seen in the spicules of the superficial sediments. (**N**) Some of the spicules buried at 23 cm showed dissolution through the axial canal, which, unlike that in the spicules of living sponges and in the superficial sediment, became free of silica.

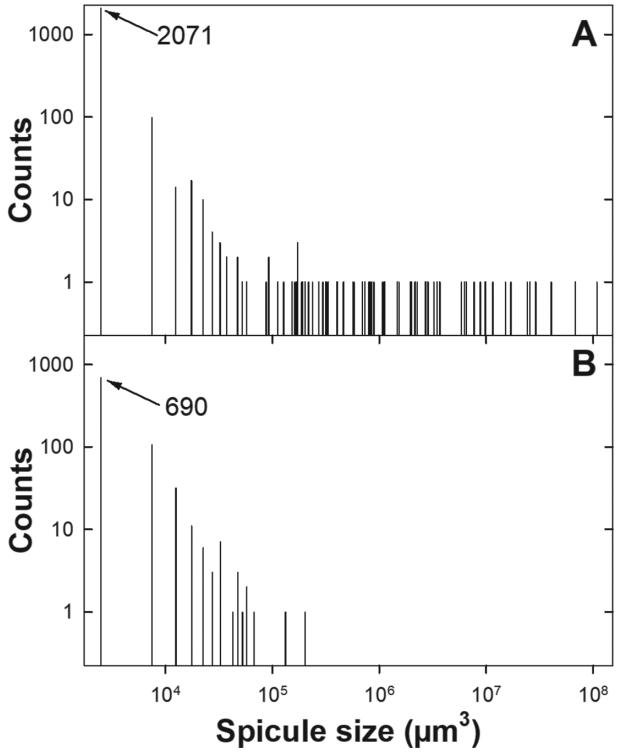

Fig 11. Size distribution of sponge spicule remains in (**A**) the superficial sediments and (**B**) at 23 burial depth. A comparison of the total number of fragments found in 30 mg of dry sediments (numbers with arrow) indicates that about half of the counts have disappeared during the burial process and that, deep in the sediments, the largest spicule fragments are indeed three orders of magnitude smaller (in volume) than in the superficial sediments. In congruence with the results of the electron microscopy study (Fig. 10), these size data suggest intense dissolution of the sponge silica during the burying process.

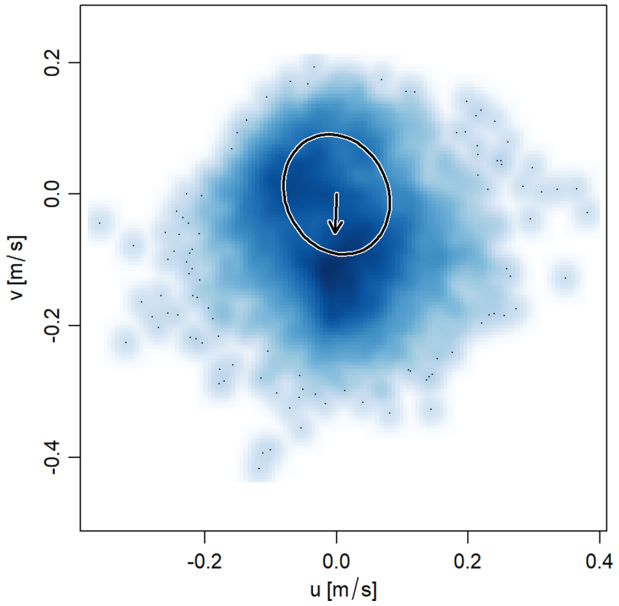

Fig 12. Horizontal flow components ($u + v$) within 3 m from bottom, as recorded by an Aquadopp 2000 kHz current meter deployed at Sambro Bank Sponge Conservation Area for 10 months (07 September 2017 to 22 June 2018).

bottom current speed was 0.12 m s^{-1} (Fig. 12) with peak currents up to 0.48 m s^{-1}. The currents alternated in direction between S-SSE and NW-NNW, in relation with semi-diurnal tides (M2). The tidal ellipse (Fig. 12) showed a relatively high eccentricity (0.76), indicating a dominant circular current. Highest currents (> 0.1 m s^{-1}) had a S-SE flow direction, while slower currents were appearing in all directions (Fig. 13). This general hydrographic pattern indicates limited movement of the bottom water and supports a scenario of relative retention on the bank and in the shallow basins of the shelf that are adjacent to the sponge aggregations. Such a hydrographic configuration would facilitate the silicic acid enrichment of the bottom water with the silicic acid efflux from the sediment of the sponge ground.

Discussion: Closing the Si cycle at the sponge grounds

From sponge biogenic silica production to deposition

Our study reveals that the *Vazella* sponge grounds consist of 6479 ± 5518 million individuals, established over an area of 2104.6 km^2. The global biogenic silica standing stock in the sponge grounds is estimated at 2.7 ± 3.7 G mol Si (Fig. 14). This standing crop consumes silicic acid at a rate of about 0.7 ± 0.7 G mol Si yr^{-1} to produce the skeleton needed for body growth (Fig. 14). The large error associated to these two figures derives from the patchy distribution of the sponges at the m^2 scale. Compared to the silicic acid consumption rates known for other sponge communities, the *Vazella* grounds can be defined as important utilizers of silicic acid (Table 2). This consumption translates entirely into skeletal biogenic silica production, which accumulates in the sponges for their lifespan. The time period needed for building such standing stock of biogenic silica is uncertain, because the average longevity of this sponge species remains unknown. A priori, it could well range from years to decades and even centuries or millennia, as known for other sponges (Ellwood et al. 2007; Jochum 2017).

After sponge death, the biogenic silica accumulated in the bodies over their lifespan is released in the form of siliceous skeletal remains (spicules). Surprisingly, when calculating the amount of sponge biogenic silica deposited to the superficial sediment of the most recent year (i.e., deposition), a deposition rate of 0.01 ± 0.008 G mol Si yr^{-1} was found (Fig. 14). Thus, there is a two order of magnitude imbalance between the annual rates of biogenic silica production and biogenic silica deposition, whereby deposition is only 1.51% of production. This leaves the question: where does the missing Si go? The disequilibrium has two plausible explanations: (1) the sponge population is currently under demographic expansion,

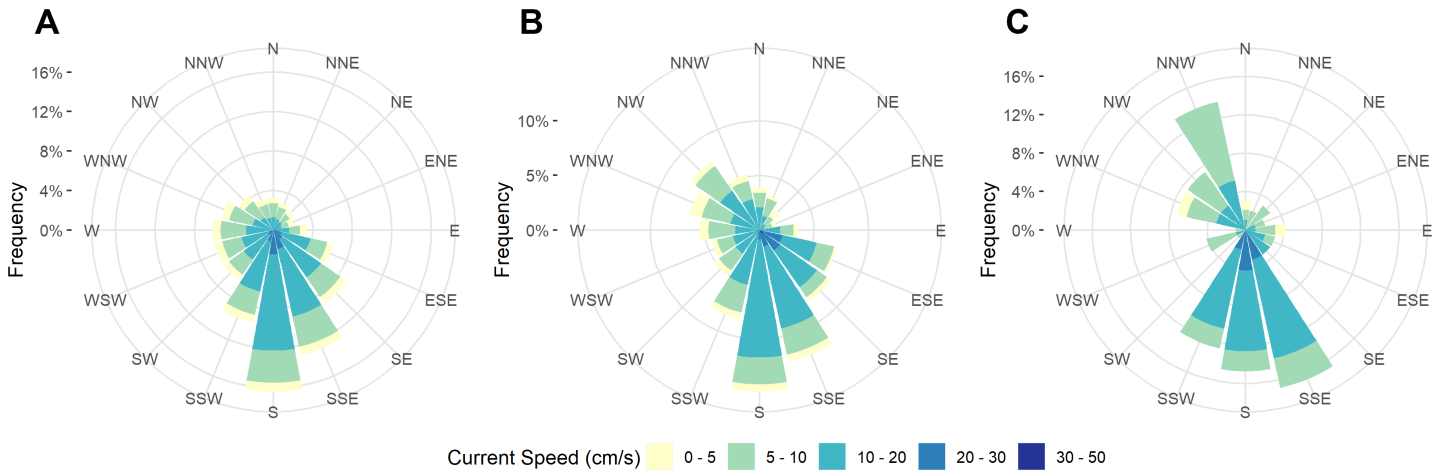

Fig 13. Current frequency plots showing the frequency and magnitude of currents within 3 m from bottom during (**A**) 10 months (07 September 2017 to 22 June 2018), (**B**) one tidal cycle (30 September 2017 to 14 October 2017), and (**C**) 1 day (09 October 2017), as recorded by an Aquadopp 2000 kHz current meter deployed at Sambro Bank Sponge Conservation Area.

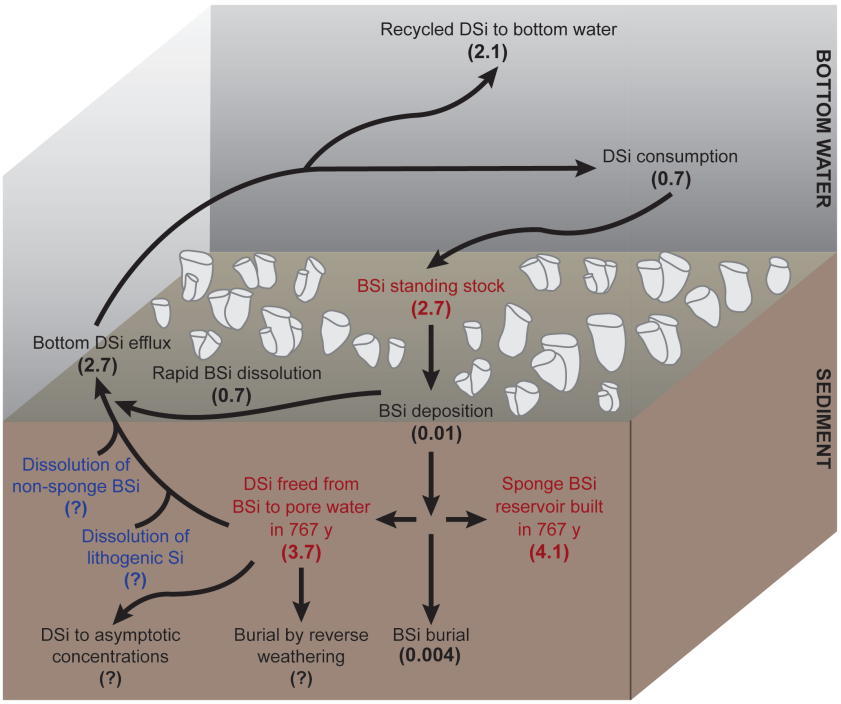

Fig 14. Scheme summarizing flux rates (in black; units are in giga mol Si yr^{-1}) and stocks (in red; units are giga mol Si) of the Si cycle across the aggregations of the hexactinellid sponge *V. pourtalesii* at the central Scotian Shelf. Silicon that is not processed through the sponges has been indicated in blue lettering. Silicic acid and biogenic silica are referred to as "DSi" and "BSi," respectively.

so that the amount of Si retained every successive year is greater, as it is retained to support the growth of the newest young individuals recruiting in the population; (2) some of the spicules of *V. pourtalesii* may dissolve rapidly after sponge death and before burial in the sediments.

Regarding the first issue, the notion that the studied sponge grounds are under demographic expansion is clearly supported by the analyses of size distribution in the aggregations (Fig. 4). From ROV observations, it can be concluded that maximum individual height in the population is about 40 cm and maximum volume about 15 liter. This maximum size of the *V. pourtalesii* individuals on the Scotian Shelf is larger than reported elsewhere over its known distribution (Tabachnick 2002), suggesting that the Scotian Shelf may be a

Table 2. Comparative summary of silicic acid (DSi) demands per m^2 and day in different sponge-dominated and diatom-dominated communities (updated from Maldonado et al. 2012). Data for the Bay of Brest come from López-Acosta et al. (2018). The densest areas of the *Vazella* ground within the closures are consuming DSi at rates that are in the same order of magnitude that the hexactinellid reefs at British Columbia (Canada) and the average of the sponge ground consumes DSi at a level similar to that of the abundant and diverse sponge community at an outer Caribbean reef.

Habitat/system	Mean DSi demand (mmol Si m^{-2} d^{-1})
Planktonic diatoms	
Coastal upwelling	90
Other coastal conditions	15
Southern Ocean	15
Open-water oceanic regions	2.3
World Ocean average	1.6–2.1
Upper continental shelf	
Bay of Brest	0.1
Outer Barrier Reef of Belize	0.9
Baltic sublittoral bottom	0.44
Mediterranean rocky bottom	0.01
Antarctic demosponge population	22.9
Deep-continental shelf	
Canadian hexactinellid reefs	3.52
Vazella ground (densest zones)	1.14
Vazella ground (average)	0.86

particularly favorable environment for this species. Given that ~ 70% of individuals found in the population monitoring were smaller than 0.2 liter (Fig. 4), the putative favorable conditions appear, in turn, to enhance reproduction and/or settlement of new recruits. Unfortunately, an approximate rate of demographic recruitment and population growth could not be predicted from the current approach. However, the magnitude of biogenic silica standing stock relative to the annual rate of silicic acid utilization indicates that (1) the current standing stock of biogenic silica in the *Vazella* grounds would require only 4 years to be generated and (2) the biogenic silica accumulation in the population would be kept at a similar pace if no biogenic silica is released from the sponge ground at any point. Although astonishing demographic shifts have been recorded in some sponge communities under decadal monitoring (Dayton 1989; Fillinger et al. 2013), our two-year survey of the *Vazella* grounds suggests that the standing stock is not growing at a pace that could account for a maintained increase in biogenic silica production of about 18.6 million kg Si yr^{-1} (i.e., 0.7 G mol Si yr^{-1}). Therefore, although the sponge population is clearly in a demographic expansion, the bulk of missing Si—expected to attain balance in the long run—cannot be satisfactorily explained by claiming a demographic situation that may be transitory. The missing Si is better accounted for by a rapid biogenic silica–silicic acid turnover in the sponge aggregations. A priori, such a turnover would involve both (a) a relatively short lifespan (i.e., in the range of years to few decades, rather than several centuries to millennia) and, more importantly, (b) a relatively rapid dissolution of the sponge spicules released to the superficial sediments and before any burial.

The idea that part of the spicules of *V. pourtalesii* rapidly dissolves into silicic acid after sponge death also appears to hold from both the electron microscopy study of the spicules in the sediment and the quantification of the sponge silica in the superficial sediments and at 23 cm depth. The idea of a rapid spicule dissolution contradicts the results of most previous studies that have investigated the dissolution of sponge spicules, which have consistently demonstrated that the siliceous skeletons of a variety of hexactinellids and demosponges are relatively resistant to dissolution—compared to diatom silica—in both seawater and alkaline solutions (Kamatani 1971; Maldonado et al. 2005; Maldonado et al. 2019). Nevertheless, the hypothesis that a rapid partial dissolution of the *V. pourtalesii* biogenic silica agrees with a previous finding by Bertolino et al. (2017), who, despite using a method of arguable accuracy to quantify rates of spicule dissolution (see Supplementary Materials in Maldonado et al. 2019), provided evidence that the spicules of the hexactinellid *Rossella racovitzae* were far less resistant to dissolution than the average known for the rest of sponges assayed to date. This could also be the case in *V. pourtalesii*. However, whereas Bertolino et al. (2017) proposed that a widening of the axial canal was the main mechanism explaining the rapid spicule dissolution, a re-examination of the pictures included in their study shows that silica delamination is visible in the micrographs published by Bertolino et al. (2017), suggesting that such process is also among the reasons for the rapid spicule dissolution in *R. racovitzae*.

From the difference between the annual rate of silicic acid consumption and the biogenic silica deposited in the sponge grounds (and after assuming negligible demographic expansion in the long run), the silicic acid recycling due to the rapid dissolution of the sponge spicules can be estimated indirectly at $652 \pm 638 \times 10^6$ mol Si yr^{-1} (Fig. 14). Such a rapid recycling of the siliceous spicules operates as a feedback mechanism that can cover, on average, 98.44% of the silicic acid annual demand in the *Vazella* grounds, facilitating the biogeochemical system of the sponge grounds to reach biogeochemical equilibrium in the long term (Fig. 14). Such a feedback mechanism would also avoid a critical dependence of the sponge grounds from silicic acid inputs associated to the sinking of primary production. Likewise, the uncovered remineralization mechanism may help to relax the competitive dominance that coastal populations of diatoms exert on siliceous shallow-

water sponges (Maldonado et al. 1999; 2011; López-Acosta et al. 2018).

Sponge biogenic silica in sediments: Dissolution, preservation, and reservoirs

Although a good portion of the annual sponge biogenic silica production appears to be recycled right after deposition and before any burial, the long-term continuity of the sponge grounds has led to a huge reservoir of sponge biogenic silica in the sediments throughout a modest—but maintained—annual deposition. More specifically, in the 767 year-old, 23 cm-high sediment column over the extension of the current sponge grounds, the estimated biogenic silica reservoir is 4.1 ± 0.6 G mol Si, some 114 million kg Si (Fig. 14). This value is even slightly higher that the biogenic silica standing stock of 2.7 ± 3.7 G mol Si in the living population (i.e., some 75.1 million kg Si, on average). The rest of the biogenic silica reservoir in the sediment is progressively dissolved back to porewater silicic acid (3.7 ± 0.6 G mol Si; that is, 103 million kg Si) and its fate impossible to be retraced back with accuracy: part of it might have experienced precipitation by reverse weathering (Ehlert et al. 2016), part of it may have already been incorporated into the water column as biologically available silicic acid, and part of it may be contributing to the asymptotic silicic acid concentrations in pore water (Fig. 14). Asymptotic silicic acid concentration in pore water of 200 μM is attained in most North-Atlantic sediments (Sarmiento and Gruber 2006) and up to 300 μM in the sediments of Emerald Basin (Andrews and Hargrave 1984).

While we were unable to empirically determine the silicic acid efflux from sediments at the sponge grounds themselves, the silicic acid efflux rate obtained by using literature data for the sediment of Emerald Basin (Andrews and Hargrave 1984) was 2.7 ± 1.2 G mol Si yr^{-1} (i.e., 75.4 kg Si yr^{-1}; Fig. 14), a figure falling within the magnitude of the other flux rates composing the Si cycle at these sponge grounds. If any, the data provided by Andrews and Hargrave (1984) are conservative. The authors concluded that the scarcity of invertebrates in the collected sediments indicated that bioturbation by burrowing invertebrates was unimportant in terms of accelerating the silicic acid efflux from the interstitial water. However, subsequent studies have demonstrated that benthic fish can play a relevant role in enhancing the silicic acid efflux, tripling silicic acid release from the superficial sediments and hindering biogenic silica preservation (Katz et al. 2009). Importantly, mixed schools of pollock and red fish (*Sebastes*), along with other demersal fish, are common at and around the *Vazella* grounds (Figs. 1A, 2A, Video S1), the activity of which could not be captured by Andrews and Hargrave's approach (1984). The abundance and biodiversity of invertebrates within the sponge ground has also been quantified to be larger than in the adjacent areas devoid of sponges (Hawkes et al. 2019). Consequently, bioturbation is expected to be a relevant factor in explaining variability in the silicic acid efflux in future studies of the *Vazella* ground sediments and elsewhere.

Implications of sponge biogenic silica recycling

The total annual silicic acid efflux from the sediments of the sponge ground was estimated at 2.7 ± 1.2 G mol Si yr^{-1} (Fig. 14). Such flux already incorporated the silicic acid contributed by the rapid partial dissolution of the spicules after deposition (i.e., 0.7 ± 0.7 G mol Si yr^{-1}), which is poorly constrained as it was indirectly estimated from the difference between the produced and deposited sponge biogenic silica. Of course, the net silicic acid efflux is also contributed in undetermined proportions by not only the dissolution of the buried sponge spicules, but also by siliceous skeletons of organisms different from sponges (e.g., diatoms, radiolarians, etc.) and by dissolution of lithogenic silicas. The magnitude of the net silicic acid efflux is large enough to trigger a feedback process that fulfills 100% of the annual silicic acid demand by the sponge grounds. After meeting sponge consumption, an additionally silicic acid pool of at least 2.0 ± 1.3 G mol Si yr^{-1} (some 57.0 million kg Si yr^{-1}) is left, which appears to end enriching the bottom water at the central Scotian Shelf with silicic acid (Fig. 14). To calculate the real rates at which the silicic acid efflux is diffusing into the bottom water mass would involve a detailed characterization of the hydrodynamics of bottom water at the Scotian Shelf, which is an extremely complex task (Petrie and Drinkwater 1993; Ohashi et al. 2009) and goes beyond the scope of the current approach. In conditions of stagnated water, the silicic acid efflux would increase the silicic acid concentration of the bottom water of the sponge grounds in 637.6 ± 284.8 and 212.5 ± 94.9 μM over a year, for a 2 m-high and a 6 m-high water column, respectively. But hydrodynamics does matter. In the opposite hypothetical scenario, that is, in the case of a steady unidirectional current flow, the silicic acid efflux from the sediments would be rapidly diluted and washed away from the sponge grounds. For instance, if the average current speed measured at 3 m from the bottom of 0.12 m s^{-1} was strongly directional, it would replace the 2 m-high water mass over the 150 km-long sponge aggregation about twice a day, diluting rapidly the silicic acid efflux. However, the current meter deployed at Sambro Bank Sponge Conservation Area detected that, while water movement has a net southern prevailing direction along the shelf, secondary northern reversions often occurred and, throughout the tidal cycle, shifts in all directions (Figs. 12, 13), revealing a dominant circular current. Such a hydrographic pattern is consistent with a scenario of slow dispersion of the silicic acid efflux from the sediments, facilitating its retention in the bottom water at the bank and in the small basins of the continental shelf adjacent to the sponge grounds, as it is reflected by summer and winter maps of silicic acid concentrations in bottom water (Fig. 4A,B). In congruence with a scenario of relative retention of the bottom water, a previous study has also described a weak anti-cyclonic gyre

that flows around the inner basins of the Scotian Shelf (Beazley et al. 2018). The stratification of the water column on the Scotian Shelf, and particularly in summer, also limits the extent of vertical mixing (Drinkwater et al. 2002). The herein described "silicic acid-rich pockets" of bottom water had already been depicted in past silicate maps of the central Scotian Shelf (Petrie et al. 1999) but, to our knowledge, their origin remained unexplained. The gathered evidence in the present study supports the notion that the sponge biogenic silica reservoir accumulated in the sediments during the existence of the sponge grounds functions as the main benthic source of silicic acid to the deep water of the central Scotian Shelf.

An alternative explanation for the co-occurrence of sponge abundance and silicic acid-enriched bottom water would be that the sponge aggregations established and prospered in those areas of the Scotian Shelf where the silicic acid concentration in the bottom water were already higher than average. If this was the case, it would be difficult to explain why the continuous silicic acid utilization by the sponge grounds is not decreasing—but rather increasing—the silicic acid concentration in the bottom water around the aggregations. Another unanswered question would be: Where does the silicic acid recycled from the abundant sponge silica go? Even more importantly, what are the causes of the elevated silicic acid concentration in the bottom water at those specific locations of the central Scotian Shelf?

Of course, we cannot discard the possibility that not al Si sources and sinks were considered in the model. It remains unknown what part of the silicic acid efflux estimated by Andrews and Hargrave (1984) would correspond to the dissolution of diatom frustules and which one to the dissolution of sponge silica. Likewise, it is known that sporadic spills on Emerald Basin of the nutrient-rich warm slope water (WSW), which resides typically in the upper slope at 300–400 m, could contribute sporadically some silicic acid to the sponge ground system (Keigwin et al. 2003; Townsend et al. 2010). However, our data strongly suggest that the sponge grounds on the Scotian Shelf, through their long-term persistence, are modifying the surrounding demersal environment—in terms of silicic acid concentration—to their own benefit. A relatively high ambient silicic acid concentration is crucial to the survival of sponges, particularly for species in which the skeleton constitutes a major component of the body, as is the case of *V. pourtalesii*. All available kinetics known for silicic acid consumption by sponges indicate that these organisms are extremely inefficient—compared to diatoms—when incorporating silicic acid from seawater with low silicic acid concentrations to build their silica skeletons. While most planktonic diatoms achieve optimal silicic acid uptake rates at an environmental silicic acid availability of about 10 μM (Paasche 1973; Conway and Harrison 1977; Martin-Jézéquel et al. 2000), to date all assayed sponges have reached their optimum at silicic acid concentrations between 75 and 150 μM (summarized in Maldonado et al. 2020). Consequently, at the relatively low silicic acid concentrations that characterize the modern ocean—10 μM as global ocean average (Nelson et al. 1995)—, the skeletal growth of siliceous sponges is chronically limited by a low silicic acid availability. This physiological inefficiency is likely an evolutionary burden inherited from the ancestral sponges having evolved their skeletal systems in the silicic acid-rich marine environments that pre-dated the ecological expansion of emergence of diatoms (Maliva et al. 1989; Maldonado et al. 1999; 2012). Consequently, the lower the silicic acid concentration in seawater, the worse to the sponges do in terms of building their necessary siliceous skeleton. By favoring comparatively higher silicic acid concentrations around the sponge grounds, the physiological stress of a chronically limited skeletal growth is alleviated, what, in the long run, facilitates the viability of the sponge ground. Indeed, many hexactinellid aggregations in the North Atlantic and Antarctic Ocean consist of rossellid sponges (Maldonado et al. 2017). Whether the rapid biogenic silica–silicic acid turnover characterizing the spicules of *V. pourtalesii* applies to other rossellids and facilitates the aggregations of other hexactinellids, in general, is a hypothesis that deserves future investigation. Interestingly, a recent study of the δ^{30} Si values characterizing the silicic acid in pore water of Greenland sediments reports an isotopic signal suggesting that the dissolution of the buried sponge biogenic silica may be significantly contributing to the interstitial silicic acid in three out of the seven studied corers (Ng et al. 2020).

Even when the silicic acid efflux may explain how the feedback system is maintained at the sponge grounds, it does not explain how the system was set initially in motion. Ultimately, the silicic acid needed to build a minimum threshold of sponge biogenic silica as standing stock should have an external origin. It is well known that Emerald Basin waters are sporadically influenced by either the nearshore cool and fresh Labrador slope waters, or the offshore warm slope waters (Keigwin et al. 2003). The latter mass of warm slope water (WSW), typically residing in the upper 300–400 m of the slope, is comparatively rich in nutrients, including silicic acid (Townsend et al. 2010). We propose that a past massive spill of WSW over the central Scotian Shelf could have favored the initial proliferation of *V. pourtalesii*, setting the system in motion.

Because silicic acid concentrations in the North Atlantic ocean are low (maximum values around 40 μM in deep waters) compared to the Pacific and Southern Oceans (maximum values over 100 μM), the long-term persistence of aggregations of heavily silicified sponges in the North Atlantic—as it is the case of *V. pourtalesii*—may depend critically on feed-back processes similar to the one identified herein. It has been measured that, on average, about half ($45.2\% \pm 27.4\%$) of the biogenic silica deposited to the sediments by all kind of siliceous sponges dissolves as silicic acid before its permanent burial (Maldonado et al. 2019). Therefore, it is likely that the

feedback mechanism here identified is operating—although with varying importance—in every benthic community where siliceous sponges abound, irrespective of the sponges being or not hexactinellids of the family Rosellidae.

Conclusions

Most of the available knowledge regarding the quantification of the biological utilization of Si in the ocean derives from investigations revolving around planktonic diatoms, which are organisms circumscribed to the photic ocean. The Si flux quantified through aggregations of hexactinellid sponges in the aphotic zone of the central Scotian Shelf provides new insights into the oceanographic and ecological implications of localized, massive biological production of biogenic silica in the aphotic ocean. Large pools of Si are transferred from the silicic acid in the water column of the continental shelf to the benthic compartment in the form of "dark biogenic silica," that is, incorporated to the skeleton of the sponges. This skeletonized Si is stored for decades in the living population. After sponge death, the skeletal pieces are deposited on the sediments and their Si may be partially recycled as silicic acid to the bottom water becoming biologically available again and partially buried in the sediments permanently. Through this biologically dominated cycling, the sponge grounds operate, on the one hand, as localized Si sinks, contributing to the global Si output from the ocean. More importantly, the biogenic silica–silicic acid turnover of the huge skeletal reservoirs stored in the sediments through centuries of biogenic silica deposition by the sponge grounds is slowly enriching the bottom water layer with silicic acid, creating silicic acid pockets of oceanographic dimension in the demersal water around the sponge aggregations. Such a biogenic silica–silicic acid turnover sustains a feedback process that facilitates the skeletal growth of the sponges and the persistence of the sponge grounds in the long run. Collectively, our results point to deep-water sponge aggregations as crucial systems to be targeted in future studies to (1) attain a more comprehensive understanding of the biological Si utilization in the aphotic ocean, and (2) to identify shared functional patterns across different types of sponge grounds.

References

Andrews, D., and B. T. Hargrave. 1984. Close interval sampling of interstitial silicate and porosity in marine sediments. Geochim. Cosmochim. Acta **48**: 711–722. doi:10.1016/0016-7037(84)90097-8

Baines, S. B., and others. 2012. Significant silicon accumulation by marine picocyanobacteria. Nat. Geosci. **5**: 886–891. doi:10.1038/ngeo1641

Beazley, L., C. Pham, F. J. Murillo, and E. Kenchington. 2017. Cruise report for the DFO/SponGES CCGS Martha L. black oceanographic Mission (MLB2017001), August 31 to September 7, 2017. p. vi + 42. Can. Tech. Rep. Fish. Aquat. Sci.

Beazley, L., and others. 2018. Predicted distribution of the glass sponge *Vazella pourtalesi* on the Scotian Shelf and its persistence in the face of climatic variability. Plos One **13**: e0205505. doi:10.1371/journal.pone.0205505

Bertolino, M., R. Cattaneo-Vietti, M. Pansini, C. Santini, and G. Bavestrello. 2017. Siliceous sponge spicule dissolution: In field experimental evidences from temperate and tropical waters. Estuar. Coast. Shelf Sci. **184**: 46–53. doi:10.1016/j.ecss.2016.10.044

Bett, B. J., and A. L. Rice. 1992. The influence of hexactinellid sponge (*Pheronema carpenteri*) spicules on the patchy distribution of macrobenthos in the porcupine Seabight (bathyal NE Atlantic). Ophelia **36**: 217–226. doi:10.1080/00785326.1992.10430372

Chu, J. W. F., M. Maldonado, G. Yahel, and S. P. Leys. 2011. Glass sponge reefs as a silicon sink. Mar. Ecol. Prog. Ser. **441**: 1–14. doi:10.3354/meps09381

Conway, H. L., and P. L. Harrison. 1977. Marine diatoms grown in chemostats under silicate or ammonium limitation. IV transient response of *Chaetoceros debilis*, *Skeletonema costatum* and *Thalassiosira gravida* to a single addition of the limiting nutrient. Mar. Biol. **43**: 33–43. doi:10.1007/bf00392569

Dayton, P. K. 1989. Interdecadal variation in an Antarctic sponge and its predator from oceanographic climate shifts. Science **245**: 1484–1486. doi:10.1126/science.245.4925.1484

Drinkwater, K. F., B. Petrie, R. G. Pettipas, M. W. Petrie, and V. Soukhotsev. 2002. Physical oceanographic conditions on the Scotian Shelf and in the Gulf of Main during 2001, p. 1–46. DFO Canadian Sciences Advisory Secretariat. Research Document. Bedford Institute of Oceanography.

Ehlert, C., and others. 2016. Stable silicon isotope signatures of marine pore waters – Biogenic opal dissolution versus authigenic clay mineral formation. Geochim. Cosmochim. Acta **191**: 102–117 https://doi.org/10.1016/j.gca.2016.07.022

Ellwood, M. J., M. Kelly, and B. Richer De Forges. 2007. Silica banding in the deep-sea lithistid sponge *Corallistes undulatus*: Investigating the potential influence of diet and environment on growth. Limnol. Oceanogr. **52**: 1865–1873. doi:10.4319/lo.2007.52.5.1865

Fillinger, L., D. Janussen, T. Lundälv, and C. Richter. 2013. Rapid glass sponge expansion after climate-induced Antarctic ice shelf collapse. Curr. Biol. **23**: 1330–1334. doi:10.1016/j.cub.2013.05.051

Hawkes, N., M. Korabik, L. Beazley, H. T. Rapp, J. R. Xavier, and E. Kenchington. 2019. Glass sponge grounds on the Scotian Shelf and their associated biodiversity. Mar. Ecol. Prog. Ser. **614**: 91–109. doi:10.3354/meps12903

Hurd, D. C. 1973. Interactions of biogenic opal, sediment and seawater in the central equatorial Pacific. Geochim.

Cosmochim. Acta **37**: 2257–2282. doi:10.1016/0016-7037(73)90103-8

Jochum, K. P., and others. 2017. Whole-ocean changes in silica and Ge/Si ratios during the Last Deglacial deduced from long-lived giant glass sponges. Geophys. Res. Lett. **44**: 11,555–511,564. doi:10.1002/2017gl073897

Johnson, C., E. Devred, B. Casault, E. Head, and J. Spry. 2017. Optical, chemical, and biological oceanographic conditions on the Scotian Shelf and in the Eastern Gulf of Maine in 2015, p. v + 53. DFO Canadian Science Advisory Secretariat Research Document. Fisheries and Oceans Canada.

Kamatani, A. 1971. Physical and chemical characteristics of biogenous silica. Mar. Biol. **8**: 89–95. doi:10.1007/BF00350922

Katz, T., and others. 2009. Groundfish overfishing, diatom decline, and the marine silica cycle: Lessons from Saanich Inlet, Canada, and the Baltic Sea cod crash. Global Biogeochem. Cycles **23**: 1–10. doi:10.1029/2008gb003416

Keigwin, L. D., J. P. Sachs, and Y. Rosenthal. 2003. A 1600-year history of the Labrador current off Nova Scotia. Climate Dynam. **21**: 53–62. doi:10.1007/s00382-003-0316-6

Kenchington, E. and others 2016. Delineation of Coral and Sponge Significant Benthic Areas in Eastern Canada Using Kernel Density Analyses and Species Distribution Models, p. vi + 178. DFO Canadian Scientific Advisory Secretariat Research Document 2016/093.

Kenchington, E., L. Beazley, and I. Yashayaev. 2017. Hudson 2016-019 International Deep Sea Science Expedition Cruise report, p. v + 55. Can. Data. Rep. Fish. Aquat. Sci.

Laguionie-Marchais, C., L. A. Kuhnz, C. L. Huffard, H. A. Ruhl, and K. L. Smith Jr. 2015. Spatial and temporal variation in sponge spicule patches at Station M, Northeast Pacific. Mar. Biol. **162**: 617–624. doi:10.1007/s00227-014-2609-1

Llopis Monferrer, N., D. Boltovskoy, P. Tréguer, M. M. Sandin, F. Not, and A. Leynaert. 2020. Estimating biogenic silica production of Rhizaria in the global ocean. Global Biogeochem. Cycles **34**: e2019GB006286. doi:10.1029/2019gb006286

López-Acosta, M., A. Leynaert, J. Grall, and M. Maldonado. 2018. Silicon consumption kinetics by marine sponges: An assessment of their role at the ecosystem level. Limnol. Oceanogr. **63**: 2508–2522. doi:10.1002/lno.10956

Mackenzie, F. T., and R. M. Garrels. 1966. Chemical mass balance between rivers and oceans. Am. J. Sci. **264**: 507–525. doi:10.2475/ajs.264.7.507

Maldonado, M., M. C. Carmona, M. J. Uriz, and A. Cruzado. 1999. Decline in Mesozoic reef-building sponges explained by silicon limitation. Nature **401**: 785–788. doi:10.1038/44560

Maldonado, M., Ma C. Carmona, Z. Velásquez, A. Puig, A. Cruzado, A. López, C. M. Young. 2005. Siliceous sponges as a silicon sink: An overlooked aspect of the benthopelagic coupling in the marine silicon cycle. Limnol. Oceanogr. **50**: 799–809. doi:10.4319/lo.2005.50.3.0799

Maldonado, M., L. Navarro, A. Grasa, A. Gonzalez, and I. Vaquerizo. 2011. Silicon uptake by sponges: A twist to understanding nutrient cycling on continental margins. Sci. Rep. **1**: 30. doi:10.1038/srep00030

Maldonado, M., M. Ribes, and F. C. Van Duyl. 2012. Nutrient fluxes through sponges: Biology, budgets, and ecological implications. Adv. Mar. Biol. **62**: 114–182. doi:10.1016/B978-0-12-394283-8.00003-5

Maldonado, M., and others. 2017. Sponge grounds as key marine habitats: A synthetic review of types, structure, functional roles, and conservation concerns, p. 145–183. *In* S. Rossi, L. Bramanti, A. Gori, and C. Orejas [eds.], Marine animal forests: The ecology of benthic biodiversity hotspots. Springer International Publishing.

Maldonado, M., M. López'Acosta, C. Sitjà, M. García-Puig, C. Galobart, G. Ercilla, A. Leynaert. 2019. Sponge skeletons as an important sink of silicon in the global oceans. Nat. Geosci. **12**: 815–822. doi:10.1038/s41561-019-0430-7

Maldonado, M., M. López-Acosta, L. Beazley, E. Kenchington, V. Koutsouveli, and A. Riesgo. 2020. Cooperation between passive and active silicon transporters clarifies the ecophysiology and evolution of biosilicification in sponges. Sci. Adv. **6**: eaba9322. doi:10.1126/sciadv.aba9322

Maliva, R. G., A. H. Knoll, and R. Siever. 1989. Secular change in chert distribution: A reflection of evolving biological participation in the silica cycle. Palaios **4**: 519–532. doi:10.2307/3514743

Marron, A., L. Cassarino, J. Hatton, P. Curnow, and K. R. Hendry. 2019. Technical note: The silicon isotopic composition of choanoflagellates: Implications for a mechanistic understanding of isotopic fractionation during biosilicification. Biogeosciences **16**: 4805–4813. doi:10.5194/bg-16-4805-2019

Martin-Jézéquel, V., M. Hildebrand, and M. A. Brzezinski. 2000. Silicon metabolism in diatoms: Implications for growth. J. Phycol. **36**: 821–840. doi:10.1046/j.1529-8817.2000.00019.x

Nelson, D. M., P. Tréguer, M. A. Brzezinski, A. Leynaert, and B. Quéguiner. 1995. Production and dissolution of biogenic silica in the ocean: Revised global estimates, comparison with regional data and relationship to biogenic sedimentation. Global Biogeochem. Cycles **9**: 359–372. doi:10.1029/95GB01070

Ng, H. C., L. Cassarino, R. A. Pickering, E. M. S. Woodward, S. J. Hammond, and K. R. Hendry. 2020. Sediment efflux of silicon on the Greenland margin and implications for the marine silicon cycle. Earth Planet. Sci. Lett. **529**: 115877. doi:10.1016/j.epsl.2019.115877

Ohashi, K., J. Sheng, K. R. Thompson, C. G. Hannah, and H. Ritchie. 2009. Numerical study of three-dimensional shelf circulation on the Scotian Shelf using a shelf circulation

model. Cont. Shelf Res. **29**: 2138–2156. doi:10.1016/j.csr.2009.08.005

Paasche, E. 1973. Silicon and the ecology of marine plankton diatoms. II. Silicate-uptake kinetics in five diatom species. Mar. Biol. **19**: 262–269. doi:10.1007/bf02097147

Petrie, B., and K. Drinkwater. 1993. Temperature and salinity variability on the Scotian Shelf and in the Gulf of Maine 1945–1990. J. Geophys. Res.: Oceans **98**: 20079–20089. doi:10.1029/93jc02191

Petrie, B., and J. Dean-Moore. 1996. Temporal and spatial scales of temperature and salinity on the Scotian Shelf, p. 45. Canadian technical report hydrography and ocean science. Fisheries and Oceans Canada.

Petrie, B., P. Yeats, and P. Strain. 1999. Nitrate, silicate and phosphate atlas for the Scotian shelf and the gulf of Maine, p. 1–96. Can. Tech. Rep. Hydrogr. Ocean. Sci. Fisheries and Oceans Canada.

Piper, D. J. W., and S. D. Fehr. 1991. Radiocarbon chronology of late Quaternary sections on the inner and middle Scotian Shelf, south of Nova Scotia, p. 321–325. Current Research. Geological Survey of Canada.

Reiswig, H. M. 1996. Redescription and placement of the rossellid genus *Vazella* gray (Hexactinellida: Lyssacinosida). Bull. Inst. R. Sci. Nat. Belg., Biol. **66**: 135–141.

Sarmiento, J., and N. Gruber. 2006. Ocean biogeochemical dynamics. Princeton Univ. Press.

Scott, D. B., P. J. Mudie, G. Vilks, and D. C. Younger. 1984. Latest Pleistocene—Holocene paleoceanographic trends on the continental margin of eastern Canada: Foraminiferal, dinoflagellate and pollen evidence. Mar. Micropaleontol. **9**: 181–218. doi:10.1016/0377-8398(84)90013-6

Schmidt, O. (1870). Grundzüge einer Spongien-Fauna des atlantischen Gebietes. (Wilhelm Engelmann: Leipzig): iii-iv, 1–88, pls I-VI.

Simpson, T. L., and B. E. Volcani. 1981. Silicon and siliceous structures in biological systems. Springer-Verlag.

Tabachnick, K. R. 2002. Family Rossellidae Schulze, 1885, p. 1441–1505. *In* J. N. A. Hooper and R. W. M. Van Soest [eds.], Systema Porifera. Kluwer Academic/Plenum Publishers.

Tenzer, R., and V. Gladkikh. 2014. Assessment of density variations of marine sediments with ocean and sediment depths. Sci. World J. **2014**: 1–9. doi:10.1155/2014/823296

Townsend, D. W., N. D. Rebuck, M. A. Thomas, L. Karp-Boss, and R. M. Gettings. 2010. A changing nutrient regime in the Gulf of Maine. Cont. Shelf Res. **30**: 820–832. doi:10.1016/j.csr.2010.01.019

Tréguer, P., D. M. Nelson, A. J. V. Bennekom, D. J. Demaster, A. Leynaert, and B. Quéguiner. 1995. The silica balance in the world ocean: A reestimate. Science **268**: 375–379. doi:10.1126/science.268.5209.375

Tréguer, P., and P. Pondaven. 2000. Silica control of carbon dioxide. Nature **406**: 358–359. doi:10.1038/35019236

Van Cappellen, P., and L. Qiu. 1997. Biogenic silica dissolution in sediments of the Southern Ocean. I. Solubility. Deep-Sea Res. II **44**: 1109–1128. doi:10.1016/S0967-0645(96)00113-0

Acknowledgments

We thank officers and crew of Canadian Coast Guard Ships *Martha L. Black* and *Hudson* as well as the engineering teams of the ROVs *Spectrum* and *ROPOS*. Celia Sitjà, Marta García-Puig and Cristina Galobart, from the CEAB-CSIC, are thanked for their help in obtaining the morphometric parameters of the sponges and the quantification of the silica in the sediments. We thank Barry MacDonald for help with logistics during sponge collection and maintenance in experimental conditions at Bedford Institute of Oceanography-Fisheries and Oceans Canada, Sarah Thompson for the analysis of the ROV ROPOS video footage, and Javier Murillo for logistic support at Bedford Institute of Oceanography-Fisheries and Oceans Canada. Zeliang Wang and Brian Petrie are thanked for critical reading, comments and suggestions on earlier versions of this manuscript. This research was completed by funds from the SponGES H2020 grant (BG-01-2015.2. Agreement Number 679849-2), from Fisheries and Oceans Canada SPERA and IGS projects to EK, and from MINECO PBS project (CTM2015-67221-R) to MM. This study is in memory of Professor Henry Reiswig, who devoted his scientific life to research on hexactinellid sponges and passed away on 7 March 2020, at age of 84, while still working on "his hexactinellids."

Conflict of Interest

None declared.

Submitted 20 September 2019
Revised 27 April 2020
Accepted 25 July 2020

Associate editor: Benjamin Van Mooy